Behaviors of the bubble, cloud and emulsion phases in a fluidized bed

Régis Andreux, Jamal Chaouki

The original publication is available at www3.interscience.wiley.com
http://dx.doi.org/10.1002/aic.11390

Behaviors of the bubble, cloud and emulsion phases in a fluidized bed

R. Andreux
Chemical Engineering Dpt.
IFP-Lyon
Solaize B.P.3, 69390 Vernaison , France

J. Chaouki
Chemical Engineering Dpt.
Ecole Polytechnique de Montréal
C.P. 6079, succ. Centre-ville, Montréal, Quebec, Canada H3C 3A7

Abstract

An intrusive bioptical probe provides radial profiles of the PDF (Probability Density Function) of the bubble, the cloud and the emulsion phases behaviors in a fluidized bed of Geldart-A particles. The fluidizing velocity ranges between 0.20 m/s and 0.80 m/s. The bed porosity, the overall averaged bubble chords and velocities are well-predicted by correlations of the literature. The cloud thickness is closely related to the bubble chord. The amount of gas traveling through the bubble phase never exceeds 15-20 % of the total gas flow rate. The averaged porosity of the bubble, the cloud and the emulsion phases is of 88-92 %, 65-70 % and 50-55 %, respectively. The reduced bubble porosity distribution obeys a constant normal law over the fluidizing velocity range. Each distribution of the reduced bubble chord and velocity, and of the reduced cloud thickness obey a constant log normal law over the fluidizing velocity range.

Key words

fluidization, experiments, particle, optical probe, bubble, cloud, emulsion

Introduction

The description of the local behaviors of bubbling gas-particle fluidized beds is of great interest for industrial process design, scale-up and troubleshooting. The regeneration zone of the Fluid Catalytic Cracking process (Figure 1) where particles of 70 μm in diameter with a density of 1500 kg/m^3 are fluidized at 700 °C and 1 barg with a superficial velocity lower than 1.0 m/s is one of the industrial applications of concern. Note that the superficial velocity sometimes reaches values higher than 1.0 m/s in such regeneration zone depending on its operating conditions. However, this topic is not studied in the present paper since such fluidized beds pertain to the turbulent regime for which the concept of bubbles is not relevant.

The state of the art of fluidized beds under different operating conditions in terms of fluidizing velocity, temperature and pressure has been widely reviewed these last years [1-2]. However, important questions remain regarding the behavior of the local structures whether they pertain to the dense phase, the cloud phase or the bubble phase. Indeed, the description of gas-particle fluidized bed hydrodynamics usually states the coexistence of two sharply distinctive phases: the particle free spherical bubble phase, and the homogeneous and viscous dense emulsion phase made of particles close to the minimum fluidizing condition state[3]. This elegant description of the hydrodynamics had led to the well-admitted successful two-phase modeling[4] widely used to simulate different types of fluidized bed reactors. However, the

boundary between the bubble phase and the emulsion phase is obviously not so straightforward: the local porosity may increase progressively from a value a little bit higher than the minimum fluidizing porosity measured in the emulsion phase[5] up to a value close to 1 measured in the center of each bubble[6-7-8]. Therefore, a local porosity threshold must be used to differentiate the bubble from the emulsion phase and to study each phase. A rigorous method has ever been proposed[9-10] to determine this threshold using a bi-optical probe which provides the probability density function of the voltage signals related to the local amount of particles in front of the probe. The local porosity was not reported but the basis of the signal processing method may have lead to high solid concentration assessments in the bubble phase that were not consistent with two-phase model assumptions. Andreux et al.[11] improved this threshold determination method and used a bi-optical probe calibrated to provide the local porosity in addition to the bubble chord, velocity and local porosity. Bubble chord and velocity in a sand particle fluidized bed operating in the bubbling regime were consistent with the Darton et al.[12] and the Davidson-Harrison[3] correlations while the bubble phase and the emulsion phase porosities were 95 % and 70 %, respectively, that are not consistent with two-phase model assumptions. In a bubbling fluidized bed of different sand particles using a single optical probe, Cui et al.[13] also found that the porosities of the bubble phase and the emulsion phase were of 90-95 % and 60-65 %, respectively. No bubbling properties were assessed since a single optical probe was used. In contrast, Kai et al.[14] used a bi-optical probe to provide the bubble velocity under various fluidizing conditions while the bubble chord was calculated combining the measured bubble velocity and the Davidson-Harrison's correlation,

i.e. assuming particle free bubbles and emulsion phase under minimum fluidizing state condition. The resulting calculated bubble chord was unrealistically 50 % higher than the column diameter while no slugging was reported.

All these experiments imply the inadequacy of the stated assumptions of the standard two-phase models regarding the bubble and the emulsion phases over the fluidizing regimes. However, these assumptions are either modified or used as they are to model gas-particle reacting fluidized beds, what is sometimes confusing: for example, the fluidized bed of the polyethylene process has ever been simulated with a two-phase model considering non empty bubbles[15] and with a three-phase model considering empty bubbles and the cloud phase[16-17-18]. Unfortunately, the cloud phase behaviors and the bubble phase porosity have been exceptionally discussed in the bubbling and turbulent fluidized bed experimental literature. The same deficiency is usually observed in the rising fluidized bed numerical literature started by Ding and Gidaspow[19], whether the formalism is eulerian[20-21-22-23-24], or lagrangian[25-26-27]. Visualization is often the major way to describe the hydrodynamics of the bubbles.

In the present work, a method is proposed to assess the full properties of all three phases in a fluidized bed of Geldart-A particles using the bi-optical probe technique:

- bubble phase : chord, velocity and porosity time-averaged values and probability functions.
- cloud phase : thickness and porosity time-averaged values and probability functions.
- emulsion phase : porosity, time-averaged fraction and interstitial gas velocity.

A mathematical formulation of the found trends is proposed.

Experimental set-up

The experiments were carried out in a 3D cold air-fluidized bed 200 mm in diameter and 1.5 m high with solids returned to freeboard region. Air (ρ=1.2 kg/m^3, μ=1.8 10^{-5} Pa.s) was introduced through a nozzle type distributor placed above a porous plate providing high pressure drop. Typical Geldart-A particles (ρ_p=1700 kg/m^3, d_p=70 μm) were fluidized between 0.20 m/s and 0.80 m/s. The static height of the bed is 30 cm.

The local instantaneous hydrodynamics were measured at 30 cm above the distributor with a bi-optical probe of 3 mm in diameter (Figure 2). The two measurement volumes were 1 mm^3 and 1.8 mm apart. Data were acquired with a sampling velocity of 15.630 Hz over 202 s. The local instantaneous voidages are obtained with a preliminary calibration of the optical signals provided by the probe.

Signal processing

Preliminary considerations

The proposed method provides:

- The chord, D_b, the velocity, U_b, and the porosity, ε_b, of each bubble.
- The thickness, T_c, and the porosity, ε_c, of each cloud.
- The averaged porosity, $\overline{\varepsilon_e}$, of the emulsion phase.
- The averaged gas flow rate through each phase.

Detailing the method

Two neighbored local transient porosity signals are required. Typical signals are shown in Figure 3.

Step 1: bubble + cloud detection

A bubble is detected if the local instantaneous porosity exceeds 95 %, as reported in the literature[6-28-8.]

A cloud is detected over a time period if the local instantaneous porosity exceeds a value higher than the pre-assumed emulsion porosity, typically 55 %, and if a bubble is detected. The bubble + cloud structure is confirmed if the cross-correlation coefficient between the top probe and the bottom probe signals is higher than 0.9 during this time period.

Step 2: determination of the emulsion-cloud, $\overline{\varepsilon_{e-c}}$, and cloud-bubble thresholds, $\overline{\varepsilon_{c-b}}$:

Plotting the cumulative probability function of the local porosity, a dense phase and a dilute phase are observed in the fluidized bed, as previously found in the literature of gas-particle fluidized beds[9-10-11-13-28]. The porosity thresholds between the emulsion and the cloud phases, $\overline{\varepsilon_{e-c}}$, and between the cloud and the bubble phases, $\overline{\varepsilon_{c-b}}$, are determined as shown in Figure 4. Note that alternate definitions of the thresholds are possible. However, we observed that the sensitivity of the measurements to the thresholds is relatively low with our definition, what is not true with others. We preferred to report this "standard" thresholds method determination, which may be the most relevant based on our experience, and which leads to time-averaged values what are consistent with well-admitted correlations, as reported later.

Step 3: determination of the phases behaviours

The averaged porosity and the fraction of the emulsion phase, $\overline{\varepsilon_e}$ and $\overline{\delta_e}$, are :

$$\overline{\varepsilon_e} = \frac{\int_{t,\varepsilon\varepsilon_{e-c}} \varepsilon dt}{\int_{t,\varepsilon\varepsilon_{e-c}} dt}, \quad \overline{\delta_e} = \frac{\int_{t,\varepsilon\varepsilon_{e-c}} dt}{\int_{t} dt}$$

where ε is the local instantaneous porosity, *dt* is the time step of acquisition.

The averaged porosity and the fraction of the cloud phase, $\overline{\varepsilon_c}$ and $\overline{\delta_c}$, are :

$$\overline{\varepsilon_c} = \frac{\int_{t,\varepsilon_{e-c}<\varepsilon<\varepsilon_{c-b}} \varepsilon dt}{\int_{t,\varepsilon_{e-c}<\varepsilon<\varepsilon_{c-b}} dt}, \quad \overline{\delta_c} = \frac{\int_{t,\varepsilon_{e-c}<\varepsilon<\varepsilon_{c-b}} dt}{\int_{t} dt}$$

The averaged porosity and the fraction of the bubble phase, $\overline{\varepsilon_b}$ and $\overline{\delta_b}$, are :

$$\overline{\varepsilon_b} = \frac{\int_{t,\varepsilon_{c-b}<\varepsilon} \varepsilon dt}{\int_{t,\varepsilon_{c-b}<\varepsilon} dt}, \quad \overline{\delta_b} = \frac{\int_{t,\varepsilon_{c-b}<\varepsilon} dt}{\int_{t} dt}$$

The chord and the velocity of each detected bubble, D_b and U_b, is determined using Fast Fourier Transform over the time period identified in step 1. One should refer to Bayle et al.[10] for more details. A similar treatment is used to determine the thickness of each detected cloud, T_c.

The averaged bed porosity, $\overline{\varepsilon_f}$, is :

$$\overline{\varepsilon_f} = \overline{\delta_e}\,\overline{\varepsilon_e} + \overline{\delta_c}\,\overline{\varepsilon_c} + \overline{\delta_b}\,\overline{\varepsilon_b} = \frac{\int_t \varepsilon.dt}{\int_t dt}$$

The time-averaged amount of gas through the bubble and the cloud phases, $\overline{\eta_{g,b}}$ and $\overline{\eta_{g,c}}$, are given by :

$$\overline{\eta_{g,b}} = \overline{\varepsilon_b U_b}\,\overline{\delta_b}$$

$$\overline{\eta_{g,c}} = \overline{\varepsilon_c U_c \delta_c}$$

Then, the time-averaged amount of gas through the emulsion, $\overline{\eta_{g,e}}$, is given by :

$$\overline{\eta_{g,e}} = U_f - \overline{\eta_{g,b}} - \overline{\eta_{g,c}}$$

where U_f is the fluidizing velocity.

The superficial gas velocity through the emulsion phase, $\overline{U_e}$, is given by :

$$\overline{U_e} = \frac{U_f - \overline{\eta_{g,b}} - \overline{\eta_{g,c}}}{1 - \overline{\delta_b} - \overline{\delta_c}}$$

Results description

A quite homogeneous radial profile of local bed porosity is observed at the lowest fluidizing velocity (Figure 5). A core-annulus structure appears when increasing the fluidizing velocity: the local porosity is nearly constant at the wall (55-60 %) while it increases in the center region of the column. The maximum value is measured at 7 cm to the wall and not in the center point. However, the overall porosity on the bed section is quite unchanged when the fluidizing velocity is higher than 0.4 m/s. It is well-predicted by the correlation of King[29] (Figure 6):

$$\overline{\varepsilon_f} = \frac{U_f + 1}{U_f + 2}$$

where $\overline{\varepsilon_f}$ is the bed porosity and U_f the fluidizing velocity.

The lowest standard deviation values of the local porosity measured in the annulus of the bed suggest a smoother fluidization phenomenon of this region compared to the core region (Figure 7). It is confirmed by the radial profiles of the bubble and the emulsion phases hold-

up that show that all the bubbles travel in the core region of the bed and that the near-wall region is only occupied by the emulsion phase (Figure 8). However, most of the bubble phase is found in the intermediary region characterized by the highest local porosity previously mentioned, and not in the centerline of the bed, perhaps because of a structure like the one described by Werther and Molerus[30] appearing. Increasing the fluidizing velocity makes the bubble phase fraction increase equally along the radius of the bed. The time-averaged values of the bubble velocity and bubble chord are nearly constant along the radius of the bed (Figure 9). The radial trends of the cloud phase averaged thickness and hold-up are similar to the radial trends of the bubble phase averaged chord and hold-up (Figure 10), what can be explained if each bubble is accompanied by a cloud and if the size of each cloud is directly related to the size of the corresponding bubble. The averaged porosities of the bubble, the cloud and the emulsion phases are nearly constant along the radial profiles whatever the range of fluidizing velocity is, and equal to 88-92 %, 65-70 %, and 50-55 %, respectively (Figure 11).

The time-averaged overall bubble chord increases from 4 cm to 5.5 cm when the fluidizing velocity increases from 0.2 m/s to 0.8 m/s (Figure 12). It is well-predicted by the correlation of Mori and Wen[31] in spite of a small overestimation of the effect of the fluidizing velocity. The ratio between the time-averaged overall cloud thickness and bubble chord remains constant and equal to 27 % over the range of fluidizing velocities. Surprisingly, the fluidizing velocity has low effect on the time-averaged overall bubble velocity. This observation implies that the added gas is not only going into the bubble phase but in either the cloud phase or the

emulsion phase when increasing the fluidizing velocity. Experiments show that the amount of gas traveling in the bubble phase quickly reaches a constant value of 15-20 % of the total gas flow rate when increasing the fluidizing velocity above 0.2 m/s (Figure 13). Simultaneously, the amount of gas through the cloud phase is divided by three, from 24 % to 8 % of the total flow rate, what explains the simultaneous increasing of the amount of gas through the emulsion phase from 60 % to 80 % of the total gas flow rate. The resulting superficial gas velocity in the emulsion phase increases exponentially and is always far higher than the minimum fluidizing velocity, U_{mf} (Figure 14). These results do not agree with two-phase model assumptions. However, such trends have ever been observed with Geldart-B particles for fluidizing velocities higher than half of the bubbling to turbulent regime transition criterion, U_c, under which $U_e = U_{mf}$ was found[11].

The amount of bed included in the cloud phase, δ_c, is always of the order of 10 % while the amount of bed included in the bubble phase slowly increases linearly:

$$\delta_b = 0.2 \times U_f$$

over the fluidizing velocity range (Figure 15). The amount of fluidized bed included in the emulsion phase, δ_e, decreases when increasing the fluidizing velocity and reaches a constant minimum value of 75 % for fluidizing velocities higher than 0.5 m/s.

The averaged cloud thickness is related to the averaged chord of the bubble phase. Indeed, it roughly equals 27 % of the averaged bubble chord over the fluidizing velocity range (Figure 16). Such behavior is half of the experimental data on single rising three-dimensional bubbles[32], with values of the order of 0.5-0.7. Thus, the cloud-phase theory determined at low

fluidizing velocity or considering a single rising bubble can not be straightly extrapolated to the bubbling and turbulent fluidization regimes.

The normalized standard deviations of the bubble porosity, $\sigma(\varepsilon_b)/\overline{\varepsilon_b}$, the bubble chord, $\sigma(D_b)/\overline{D_b}$, the bubble velocity, $\sigma(U_b)/\overline{U_b}$, and the cloud thickness, $\sigma(T_c)/\overline{T_c}$, are constant over the fluidizing velocity range : 23 %, 90 %, 70 % and 80 %, respectively (Figures 17-18). Thus, the dispersion of the bubbling behaviors is quite high. Consequently, using the averaged values may sometimes not be sufficient to model the bubbling phenomenon of reacting fluidized beds.

Fortunately, the present work shows that the reduced probability function of each bubbling behavior can be modeled as a constant probability function over the fluidizing velocity range:

- The reduced probability distributions of the bubble porosity, $\left(\varepsilon_b - \overline{\varepsilon_b}\right)/\sigma(\varepsilon_b)$, obey a single normal law (Figure 19).
- Each reduced probability distribution of the bubble velocity, $\left(U_b - \overline{U_b}\right)/\sigma(U_b)$, the bubble chord, $\left(D_b - \overline{D_b}\right)/\sigma(D_b)$, and the cloud thickness, $\left(T_c - \overline{T_c}\right)/\sigma(T_c)$, obey a single lognormal law (Figures 20-22).

Furthermore, the porosity of the cloud-phase can be considered as constant since its standard deviation is always lower than 3 % of the averaged value.

Mathematical formulation of the phase properties

Bubble phase:

The probability function of the bubble velocity is given by a log normal law:

$$f(U_b)=\frac{1}{a\sqrt{2\pi}U_b}\exp\left(-\frac{1}{2}\left(\frac{\ln U_b-b}{a}\right)^2\right)$$

where the parameters a and b are calculated using the mean and standard deviation bubble velocity values as:

$$\begin{cases}\overline{U_b}=e^{b+a^2/2}\\ \sigma(U_b)=e^{2b+a^2}\left(e^{a^2}-1\right)\end{cases}$$

supplemented with the Davidson-Harrison correlation[3] and the results found in this paper:

$$\begin{cases}\overline{U_b}=U_f-U_{mf}+0.711\sqrt{g.\overline{D_b}}\\ \sigma(U_b)=0.70\times\overline{U_b}\\ \text{Max amount of gas in the bubble - phase: } \overline{\delta_b\varepsilon_b U_b}<0.15U_f\end{cases}$$

The probability function of the bubble chord is given by a log normal law:

$$f(D_b)=\frac{1}{a\sqrt{2\pi}D_b}\exp\left(-\frac{1}{2}\left(\frac{\ln D_b-b}{a}\right)^2\right)$$

where the parameters a and b are calculated using the mean and standard deviation bubble velocity values as:

$$\begin{cases}\overline{D_b}=e^{b+a^2/2}\\ \sigma(D_b)=e^{2b+a^2}\left(e^{a^2}-1\right)\end{cases}$$

supplemented with the Mori-Wen correlation[31] and the results found in this paper:

$$\begin{cases}\overline{D_b}=\overline{D_{bm}}-\left(\overline{D_{bm}}-\overline{D_{b0}}\right)e^{-0.3h/D_t}\\ \overline{D_{b0}}=0.0376\left(U_f-U_{mf}\right)^2,\ \overline{D_{bm}}=0.652\left(S\left(U_f-U_{mf}\right)\right)^{2/5}\\ \sigma(D_b)=0.90\times\overline{D_b}\end{cases}$$

The probability function of the bubble porosity is given by a normal law:

$$f(\varepsilon_b)=\frac{1}{\sigma(\varepsilon_b)\sqrt{2\pi}}\exp\left(-\frac{1}{2}\left(\frac{\varepsilon_b-\overline{\varepsilon_b}}{\sigma(\varepsilon_b)}\right)^2\right)$$

supplemented with the results found in this pape :

$$\begin{cases}\overline{\varepsilon_b}=90\\ \sigma(\varepsilon_b)=0.23\times\overline{\varepsilon_b}\end{cases}$$

The bubble phase voidage is function of the fluidizing velocity: $\delta_b=0.2\times U_f$

Cloud phase:

The probability function of the cloud thickness is given by a log normal law:

$$f(T_c)=\frac{1}{a\sqrt{2\pi}T_c}\exp\left(-\frac{1}{2}\left(\frac{\ln T_c-b}{a}\right)^2\right)$$

where the parameters a and b are calculated using the mean and standard deviation cloud thickness values as:

$$\begin{cases}\overline{T_c}=e^{b+a^2/2}\\ \sigma(T_c)=e^{2b+a^2}\left(e^{a^2}-1\right)\end{cases}$$

supplemented with the results found in this paper:

$$\begin{cases}\overline{T_c}=0.27\times\overline{D_b}\\ \sigma(T_c)=0.80\times\overline{T_c}\end{cases}$$

The averaged cloud porosity is constant: $\overline{\varepsilon_c}=67.5\%$. The cloud velocity is that of the bubble to which it is attached: $U_c=U_b$. The averaged cloud phase fraction is constant: $\overline{\delta_c}=10$.

Emulsion phase:

The averaged emulsion porosity is equal to the minimum bubbling porosity, ε_{mb} .

The emulsion phase voidage is given by $\overline{\delta_e}=1-\overline{\delta_b}-\overline{\delta_c}$.

Conclusion

Extensive experiments are performed to investigate the bubbling properties in a fluidized bed of typical Geldart-A particles using a bi-optical probe.

The probability distributions of the following properties are assessed:

- the chord, velocity and porosity of the bubble phase.
- the thickness and porosity of the cloud phase.

The averaged bed and emulsion phase porosity, the fraction of all three phases, the amount of gas and the interstitial gas velocity in the emulsion phase are assessed. We observe the following:

- The averaged bed porosity is well-predicted by King's correlation[29].
- The averaged bubble chord is well-predicted by the correlation of Mori and Wen[31].
- The averaged bubble velocity is not well-predicted by the correlation of Davidson and Harrison[3] at fluidizing velocity above 0.2-0.3 m/s.
- The amount of gas traveling through the bubble phase quickly reaches a constant value of 15-20 % of the total gas flow rate when increasing the fluidizing velocity above 0.2 m/s, what explains the observed bubble velocity ceiling.
- Increasing the fluidizing velocity makes the smaller clouds be attached to the faster bubbles. Indeed, the amount of gas traveling through the cloud phase decreases while the cloud phase fraction and the cloud phase velocity are constant when increasing the fluidizing velocity.

- Bubbles are not free of particles. The averaged porosity of the bubble phase is of 88-92 % over the fluidizing velocity range.
- The averaged porosity of the cloud and the emulsion phases are of 65-70 % and 50-55 %, respectively, over the fluidizing velocity range.
- The normalized standard deviation values of the bubble chord and velocity and of the cloud thickness are constant over the fluidizing velocity range : 23 %, 90 %, 70 % and 80 %, respectively.
- The reduced bubble porosity distribution obeys a single normal law over the fluidizing velocity range.
- Each distribution of the reduced bubble chord and velocity, and of the reduced cloud thickness obey a constant log normal law over the fluidizing velocity range.
- The cloud porosity is mono distributed.

The major modeling implication of our results may be the accurate predictions of the hydrodynamics behaviors using the standard two-phase modeling coupled with a Monte-Carlo probabilistic method supplemented with the correlations we propose. Such approach could be compared to the Reynolds decomposition used in fluid dynamics and the theory of turbulence to separate the time-average and time-fluctuating parts of a quantity, and may be coupled with a chemical kinetics model to improve industrial fluidized bed reactors modeling.

Nomenclature

Roman letter

D_b Bubble chord (m)

d_p Particle diameter (μm)

dt Time step of the acquired signal (s)

r Radial position (m)

R Column radius (m)

T_c Cloud thickness (m)

U_b Bubble velocity (m)

U_c Bubbling to turbulent regime transition criterion (m/s)

U_f Fluidizing velocity (m/s)

U_{mb} Minimum bubbling velocity (m/s)

U_{mf} Minimum fluidizing velocity (m/s)

Greek letter

δ_b Fraction of the bubble phase (m^3/m^3).

δ_c Fraction of the cloud phase (m^3/m^3).

δ_e Fraction of the emulsion phase (m^3/m^3).

ε Local porosity (m^3/m^3).

ε_b Porosity of a bubble (m^3/m^3).

ε_c Porosity of a cloud (m^3/m^3).

$\varepsilon_{c\text{-}b}$ Porosity threshold between the cloud and the bubble phases (m^3/m^3).

ε_e Porosity of the emulsion phase (m^3/m^3).

$\varepsilon_{e\text{-}c}$ Porosity threshold between the emulsion and the cloud phases (m^3/m^3).

ε_f Porosity of the bed (m^3/m^3).

ε_{mb} Porosity of the bed at minimal bubbling velocity (m^3/m^3).

ε_{mf} Porosity of the bed at minimal fluidizing velocity (m^3/m^3).

$\eta_{g,b}$ Amount of gas through a the bubble phase (m/s)

$\eta_{g,c}$ Amount of gas through a the cloud phase (m/s)

$\eta_{g,e}$ Amount of gas through a the emulsion phase (m/s)

μ Gas dynamic viscosity (Pa.s).

ρ Gas density (kg/m^3).

ρ_p Particle density (kg/m^3).

$\sigma(x)$ Standard deviation of x (dimension of x)

Superscript

$\bar{}$ Time-averaged value

References

1. Bi HT, Ellis N, Abba IA, Grace JR. A state-of-the art review of gas-solid turbulent fluidization. Chem. Eng. Sci. 2000;55:4789-4825.
2. Yates JG. Effects of temperature and pressure on gas-solid fluidization. Chem. Eng. Sci. 1996;51(2):167-205.
3. Davidson JF, Harrison D. Fluidized Particles, Cambridge University Press, Cambridge, UK. 1963

4. Kato K, Wu CY. Bubble assemblage model for fluidised bed catalytic reactor. Chem. Eng. Sci. 1969;24:1351-1369.
5. Formisani B, Girimonte R, Pataro G. The influence of operating temperature on the dense phase properties of bubbling fluidized beds of solids. Powder Techn. 2002;125:28-38.
6. Yates JG, Cheesman DJ. Voidage variations in the regions surrounding a rising bubble in a fluidized bed, AIChE Symp. Series 1992;289(88):34-39.
7. Yates JG, Cheesman DJ, Lettieri P, Newton D. X-Ray analysis of fluidized beds and other multiphase systems, Kona 2002;20:133-143.
8. McKeen T, Pugsley T. Simulation and experimental validation of a freely bubbling bed of FCC catalyst, Powder Techn. 2003;129:139-152.
9. Smith M, Bayle J, Gauthier T. Bubble flow study in a turbulent FCC fluidized bed, EFCE, European Congress of Chemical Engineering , 2nd, Montpellier, Oct. 5-7 1999, p. 47, Paper C5.8.3.
10. Bayle J, Mege P, Gauthier T. Dispersion of bubble flow properties in a turbulent FCC fluidized bed, Proc of 10th Engineering Foundation Conference, Fluidization X,2001. Kwauk M et al., eds. Beijing, China : 125-132.
11. Andreux R, Gauthier T, Chaouki J, Simonin O. New description of fluidization regimes, AIChE J. 2005;51(4):1125-1130.
12. Darton DC, Lanauze RD, Davidson JF, Harrison D. Bubble growth due to coalescence in fluidized beds, Trans. Inst. Chem. Eng. 1977;55:274-280.

13. Cui H, Mostoufi N, Chaouki J. Characterization of dynamic gas-solid distribution in fluidized beds, Chem. Eng. J. 2000;79:133-143.

14. Kai T, Imamura T, Takahashi T. Hydrodynamics influences on mass transfer between bubble and emulsion phases in a fine particle fluidized bed, Powder Techn. 1995;83:105-110.

15. Kiashemshaki A, Mostoufi N, Sotudeh-Gharebagh R. Two-phase modeling of a gas phase polyethylene fluidized bed reactor, Chem. Eng. Sc. 2006;61:3997-4006.

16. El-Halwagi MM, El-Rifai MA. Mathematical modeling of catalytic fluidized-bed reactors-1. The multistage three-phase model, Chem. Eng. Sci. 1988;43:2477-2489.

17. Hatzantonis H, Yiannoulakis H, Yiagopoulos A, Kiparissides C. Recent developments in modeling gas-phase catalyzed olefin polymerization fluidized-bed reactors : the effect of bubble size variation on the reactor's performance, Chem. Eng. Sci. 2000;55:3237-3259.

18. Grosso WE, Chiovetta MG. Modeling a fluidized bed reactor for the catalytic polymerization of ethylene: particle size distribution effects, Latin American Applied Research 2005;35:67-76.

19. Ding J, Gidaspow D. A bubbling fluidization model using kinetic theory of granular flow, AIChE J. 1990;36(4):523-538.

20. Laux H, Johansen ST. Computer simulation of bubble formation in a gas-fluidized bed, 1998, Fluidization IX.

21. Schmidt A, Renz U. Eulerian computation of heat transfer in fluidized beds, Chem. Eng. Sci. 1999;54:5515-5522.

22. Guenther S, Syamlal M. The effect of numerical diffusion on isolated bubbles in a gas-solid fluidized bed, Powder Techn. 2001;116:142-154.

23. Pain CC, Mansoorzadeh S, Gomes JML, de Oliveira CRE. A numerical investigation of bubbling gas-solid fluidized bed dynamics in 2-D geometries, Powder Techn. 2002;128:56-77.

24. Gao K, Wu J, Wang Y, Zhang DK. Bubble dynamics and its effects on the performance of a jet fluidized bed gasifier simulated using CFD, Fuel 2006;85:1221-1231.

25. Kawaguchi T, Miyoshi A, Tanaka T, Tsuji Y. Discrete particle analysis of 2D pulsating fluidized bed, ICMF2001.

26. Lie J, Kuipers JAM. Effect of pressure on gas-solid flow behavior in dense gas-fluidized beds : a discrete particle simulation study, Powder Techn. 2002;127:173-184.

27. Wu CL, Zhan JM, Li YS, Lam KS. Dense particulate flow model on unstructured mesh, Chem. Eng. Sci. 2006;61:5726-5741.

28. Cui H, Mostoufi N, Chaouki J. Gas and solids between dynamic bubble and emulsion in gas-fluidized beds, Powder Techn. 2001;120:12-20.

29. King DF. Estimation of dense bed voidage in fast and slow fluidized beds of FCC catalyst. In: Grace JR, Shemilt LW, Bergougnou MA. Fluidization vol. VI. New York: Engng. Foundation, 1989:1–8.

30. Werther J, Molerus O. the local structure of gas fluidized beds : Part II : The spatial distribution of bubble. Int. J. Multiphase Flow. 1973;1:123-138.

31. Mori S, Wen CY. Fluidization Technology.Washington: Kealrns DL, Ed., Hemisphere Pub. Corp., 1976: 179.

32. Kunii D, Levenspiel O. Fluidization Engineering, 2nd ed.; Butterworth-Helnemann : Boston, 1991.

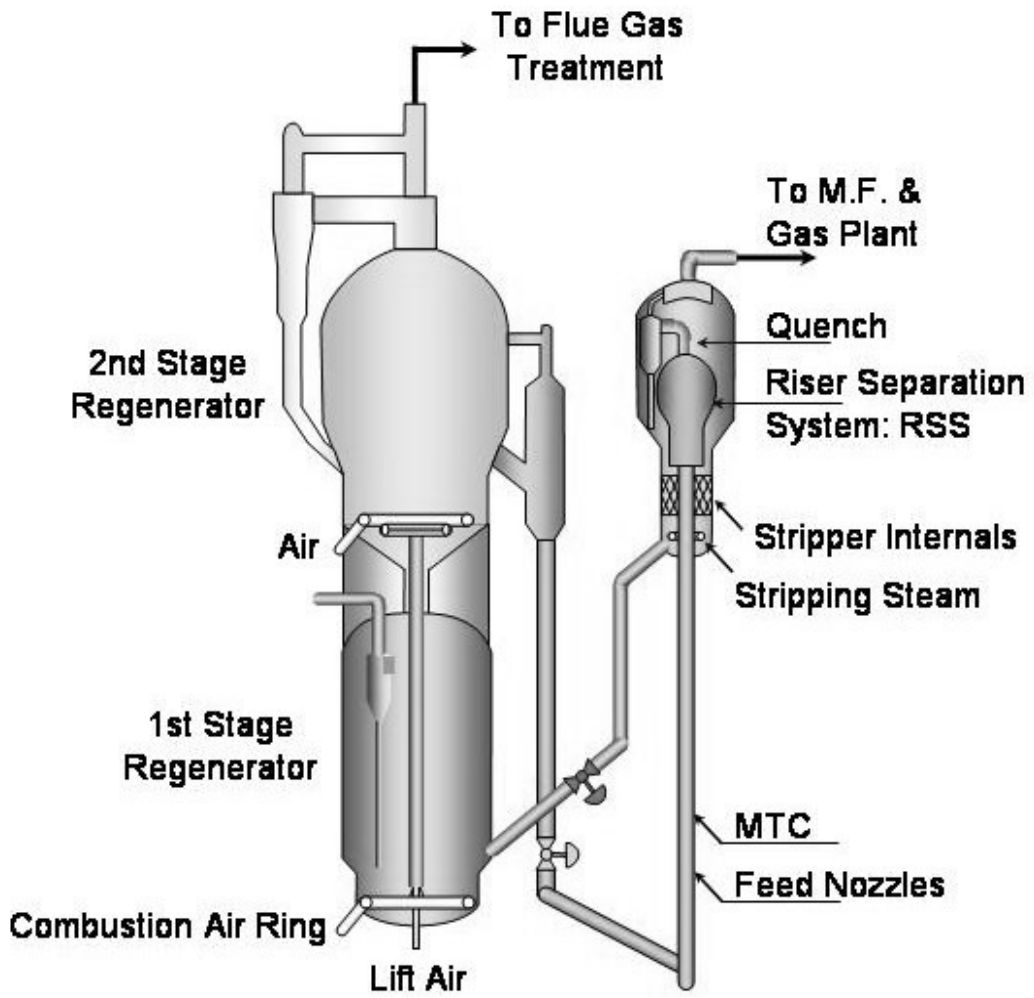

Figure 1: The R2R resid Fluid Catalytic Cracking process (Axens – IFP – Stone & Webster Inc. – TOTAL Technology).

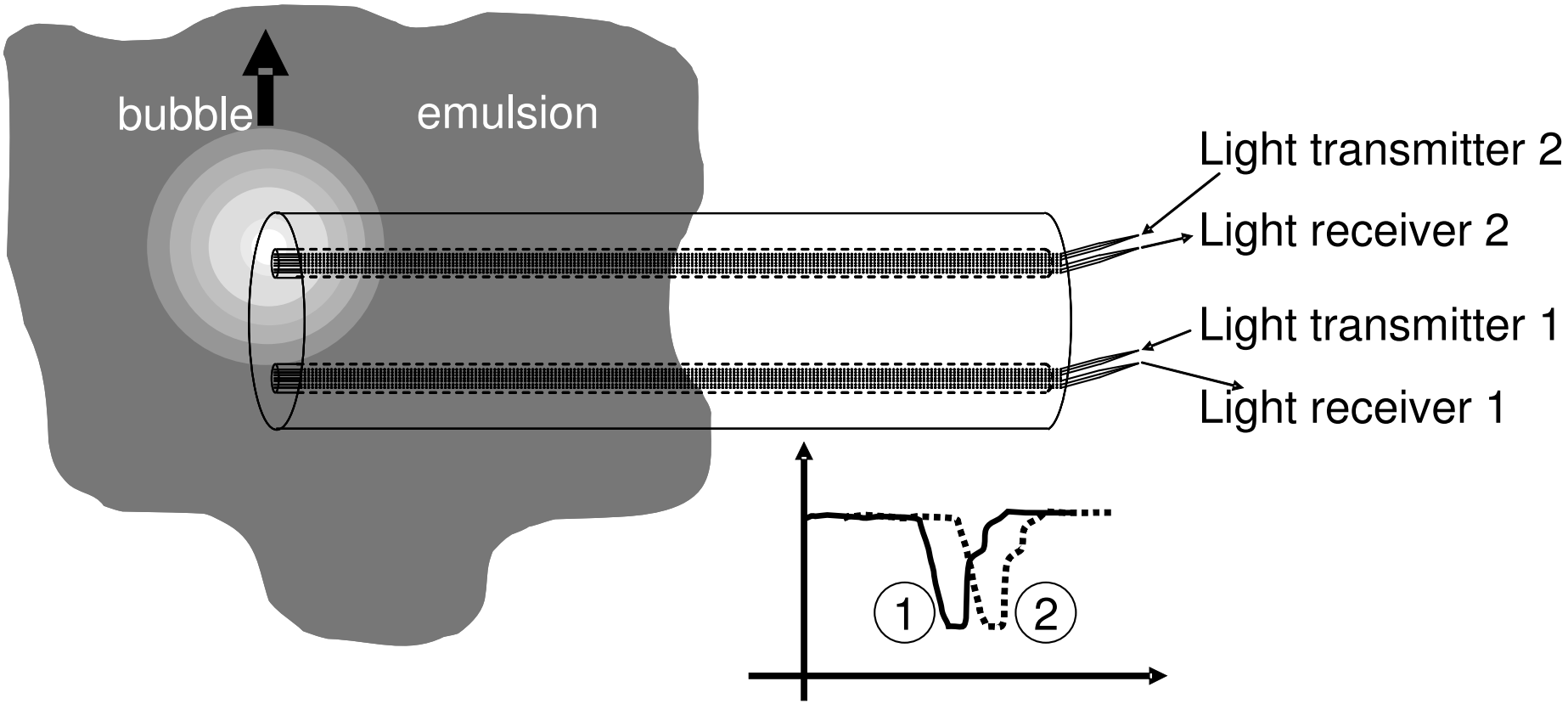

Figure 2: Schema of the bi-optical probe.

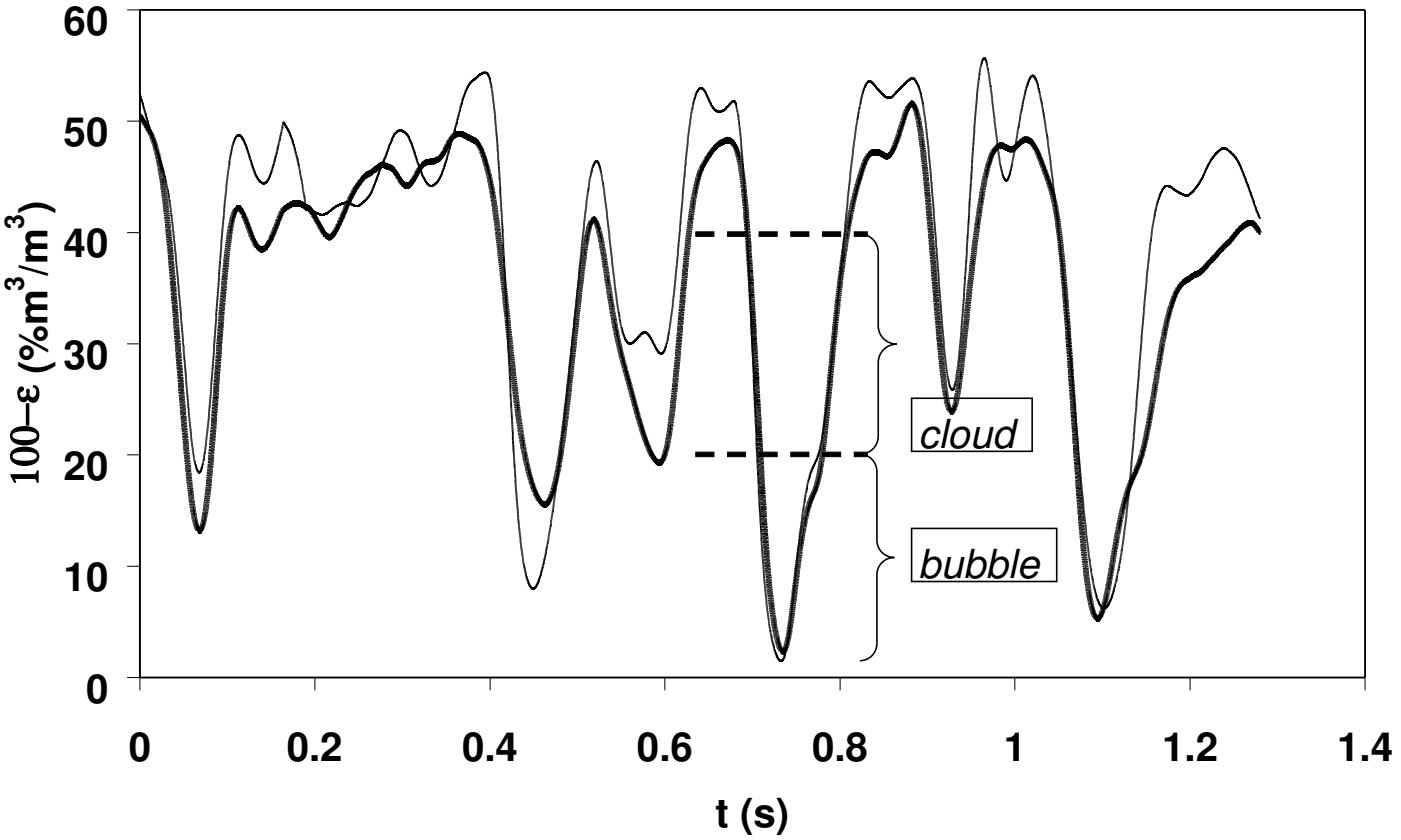

Figure 3 : Typical signal to be processed.

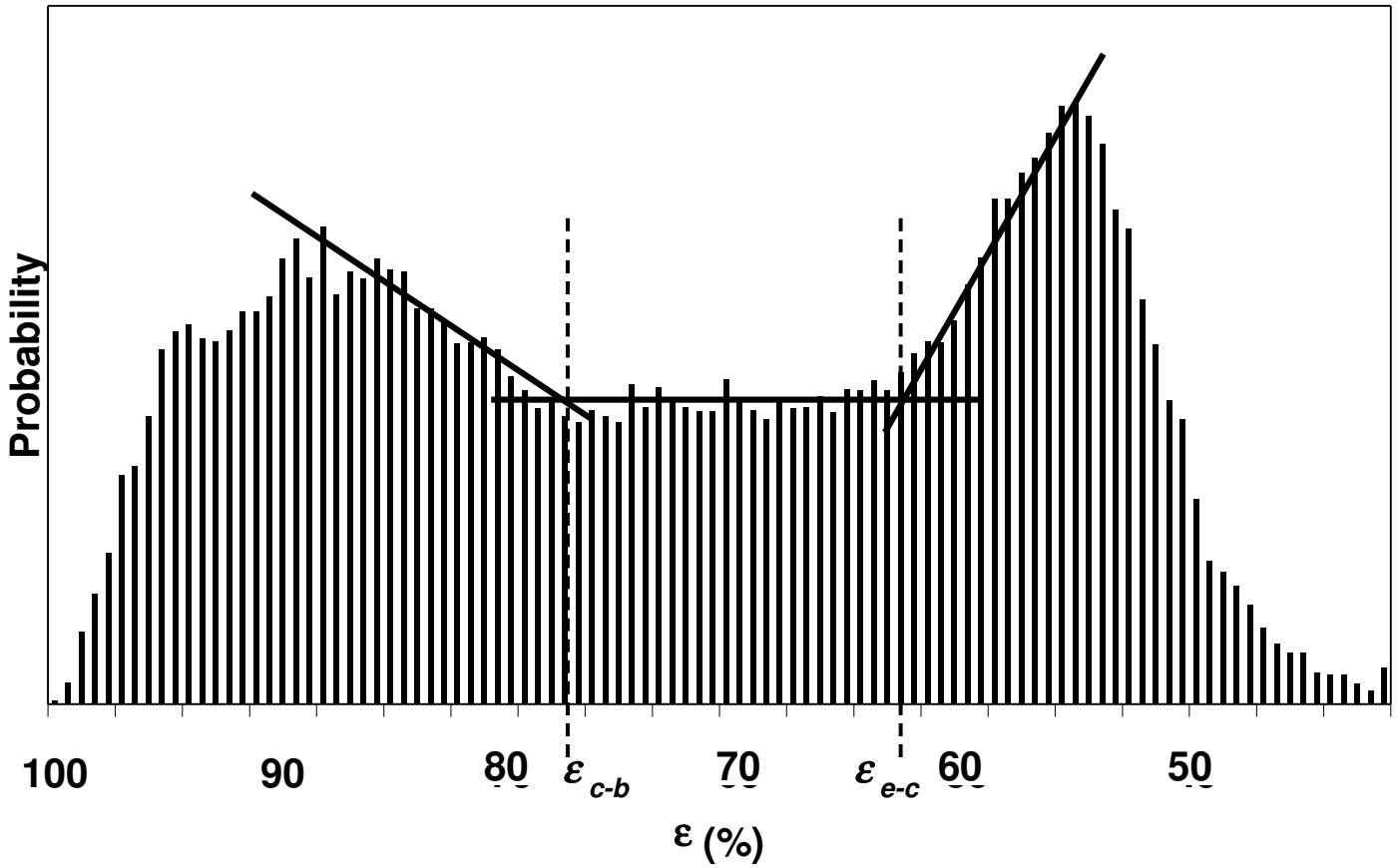

Figure 4 : Thresholds determination using the distribution of the local voidage acquired with the bi-optical probe.

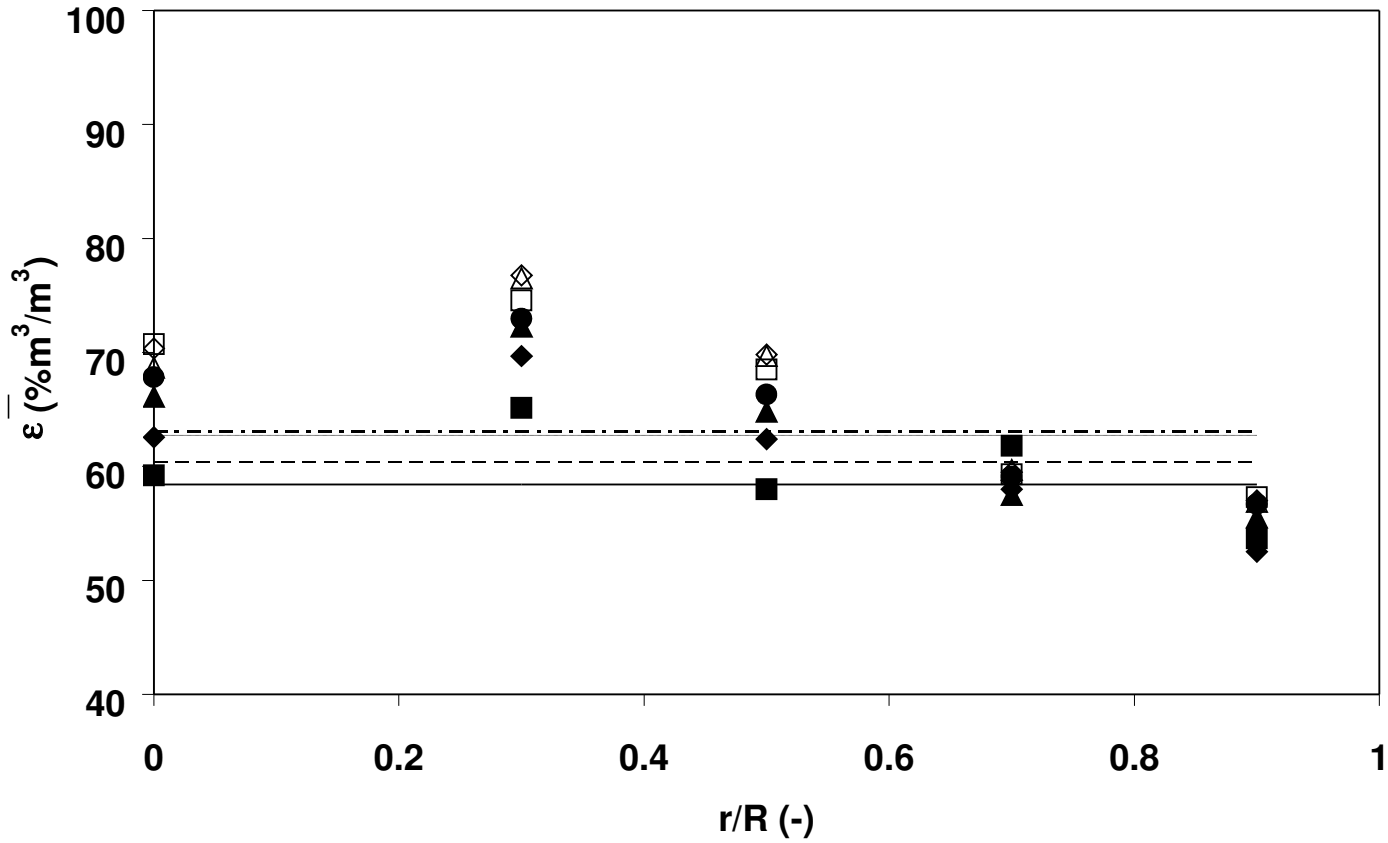

Figure 5 : Radial profiles of the time-averaged local porosity at 30 cm above the distributor (0.2 m/s ■. 0.3 m/s ◆. 0.4 m/s ▲. 0.5 m/s ●. 0.6 m/s ◇. 0.7 m/s □. 0.8 m/s ◈). Effect of the fluidizing velocity, U_f.

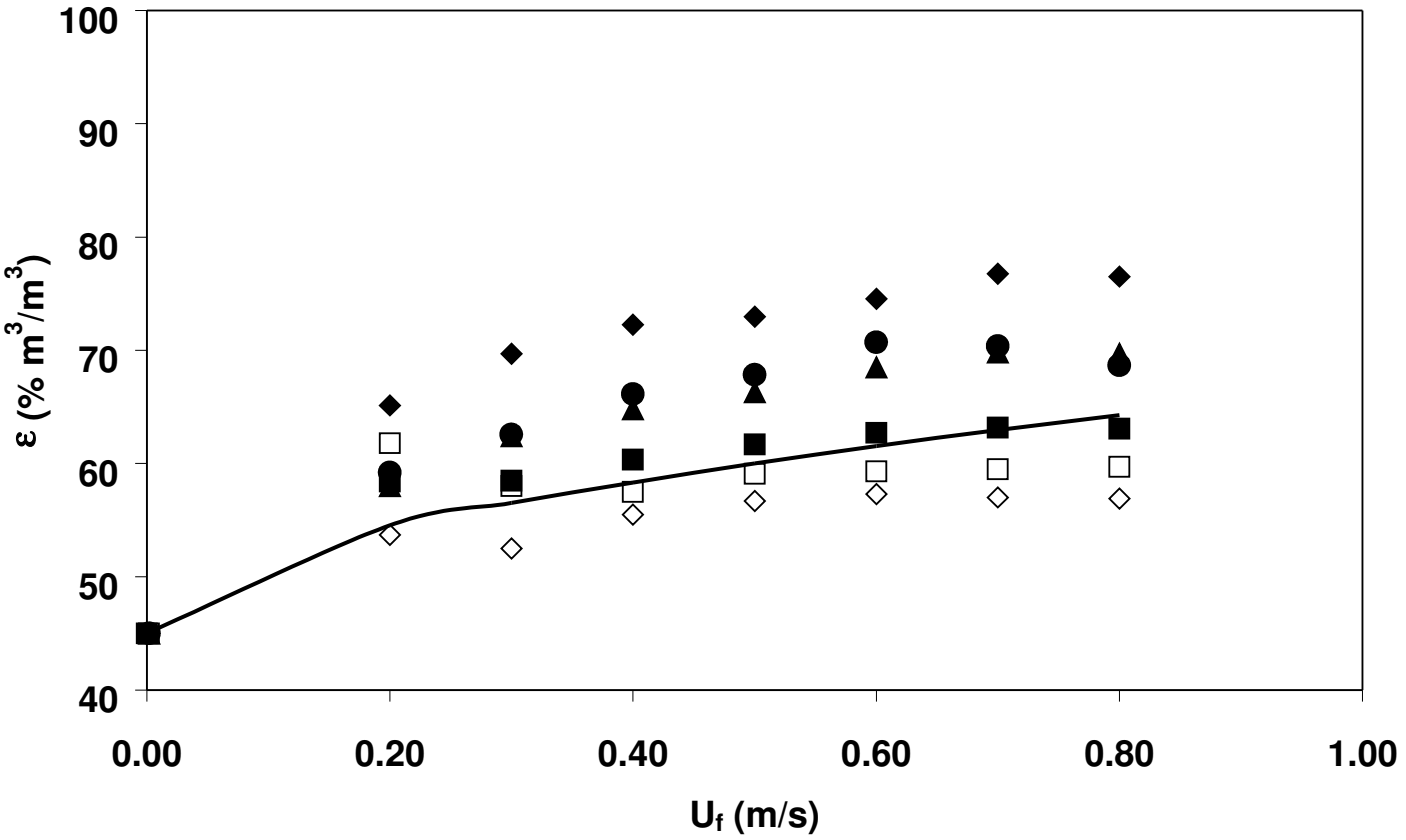

Figure 6 : Time-averaged local porosity at 30 cm above the distributor at different radial position (3 cm to the wall ◆. 5 cm to the wall 娚. center position □. 7 cm to the wall 撽. 9 cm to the wall 斂). Comparison between the overall time-average porosity of the porosity (亂) and the correlation of King, 1989 (—). Effect of the fluidizing velocity, U_f.

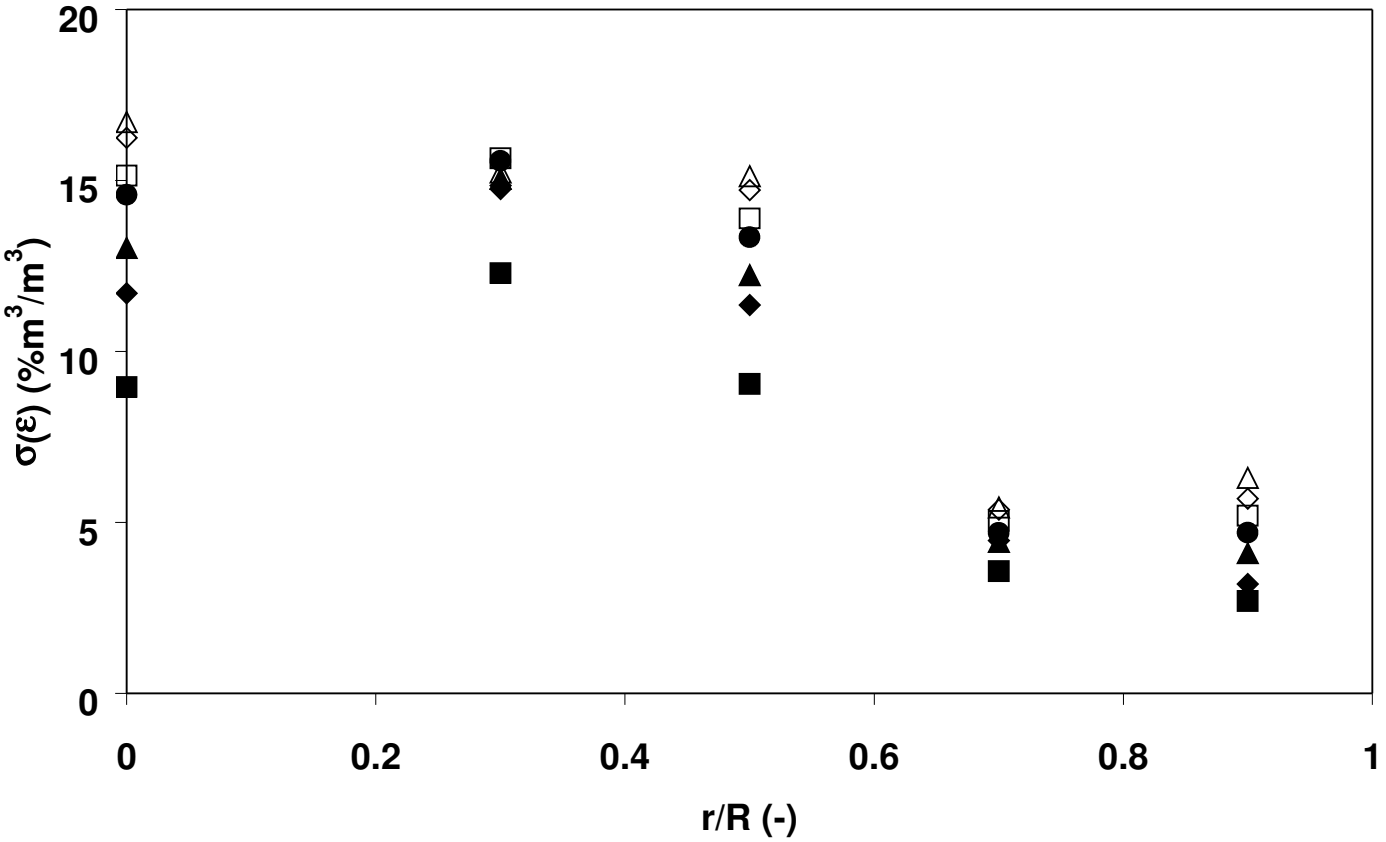

Figure 7 : Radial profiles of the standard deviation of the local porosity at 30 cm above the distributor (0.2 m/s □. 0.3 m/s ◆. 0.4 m/s 娚. 0.5 m/s ●. 0.6 m/s 撽. 0.7 m/s 歟. 0.8 m/s △). Effect of the fluidizing velocity, U_f.

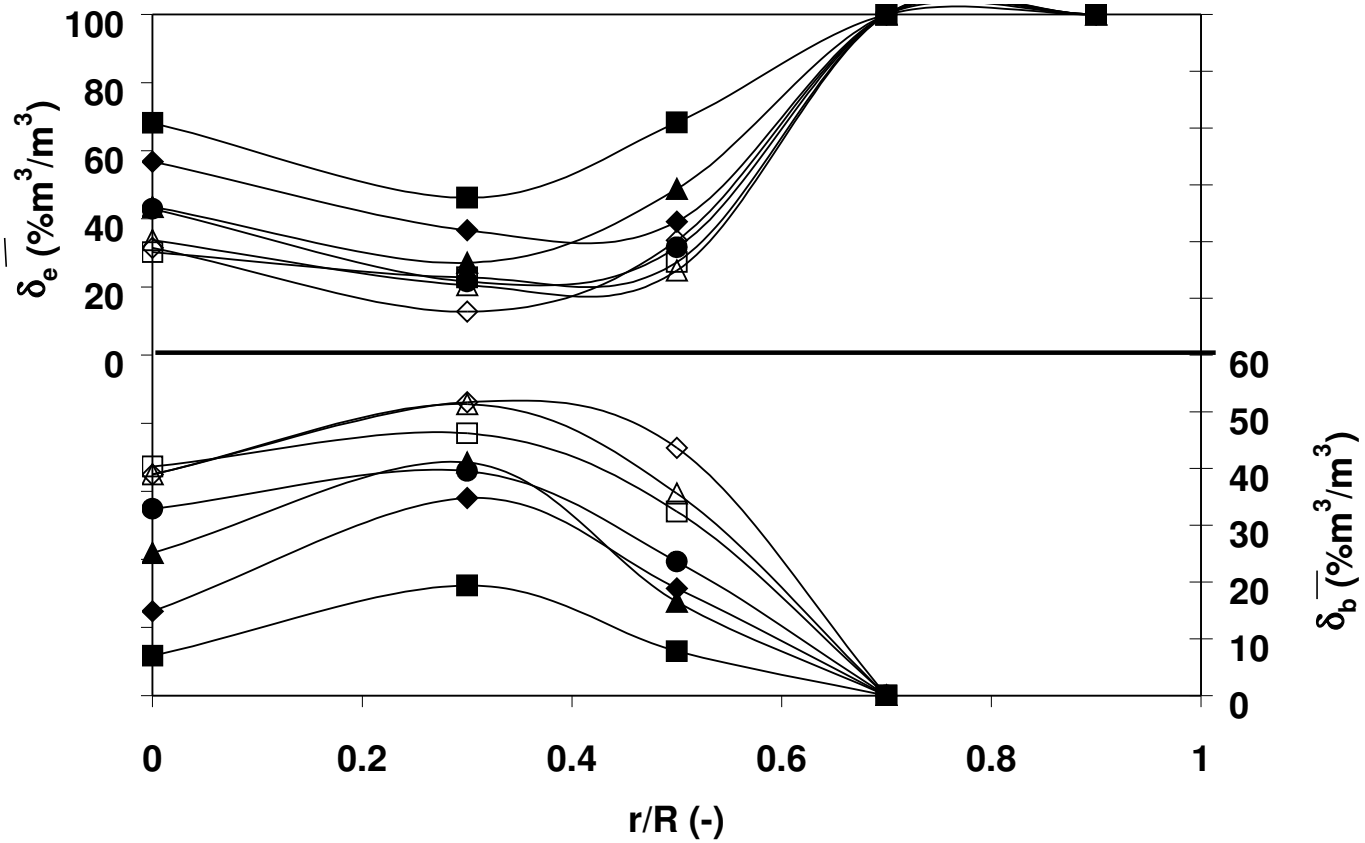

Figure 8 : Radial profiles of the emulsion and bubble phases fraction at 30 cm above the distributor (0.2 m/s ■. 0.3 m/s ◆. 0.4 m/s 妍. 0.5 m/s ■. 0.6 m/s 撽. 0.7 m/s 歟. 0.8 m/s △). Effect of the fluidizing velocity, U_f.

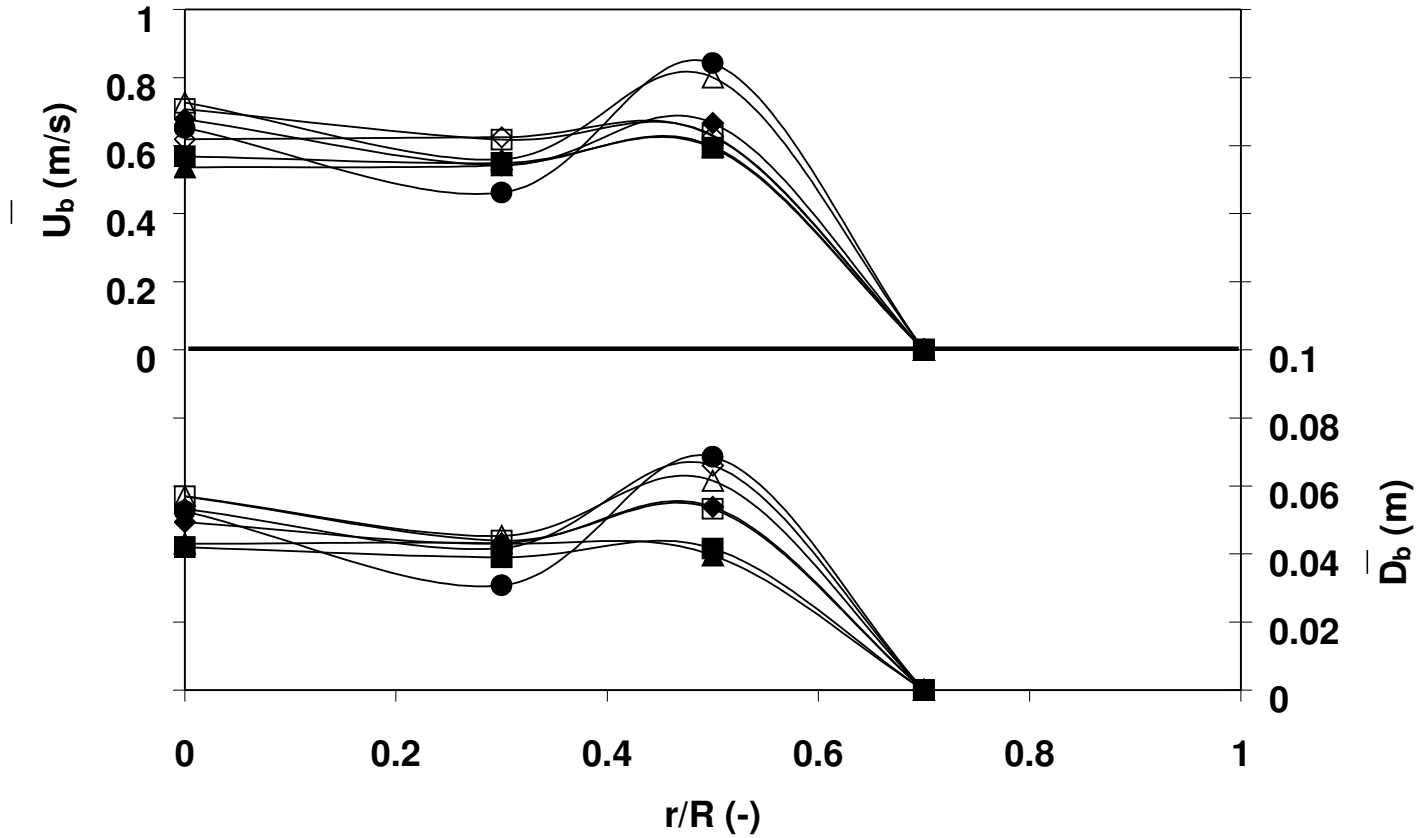

Figure 9: Radial profiles of the time-averaged bubble velocity and chord at 30 cm above the distributor (0.2 m/s □. 0.3 m/s ◆. 0.4 m/s 姍. 0.5 m/s □. 0.6 m/s 撿. 0.7 m/s 數. 0.8 m/s △). Effect of the fluidizing velocity, U_f.

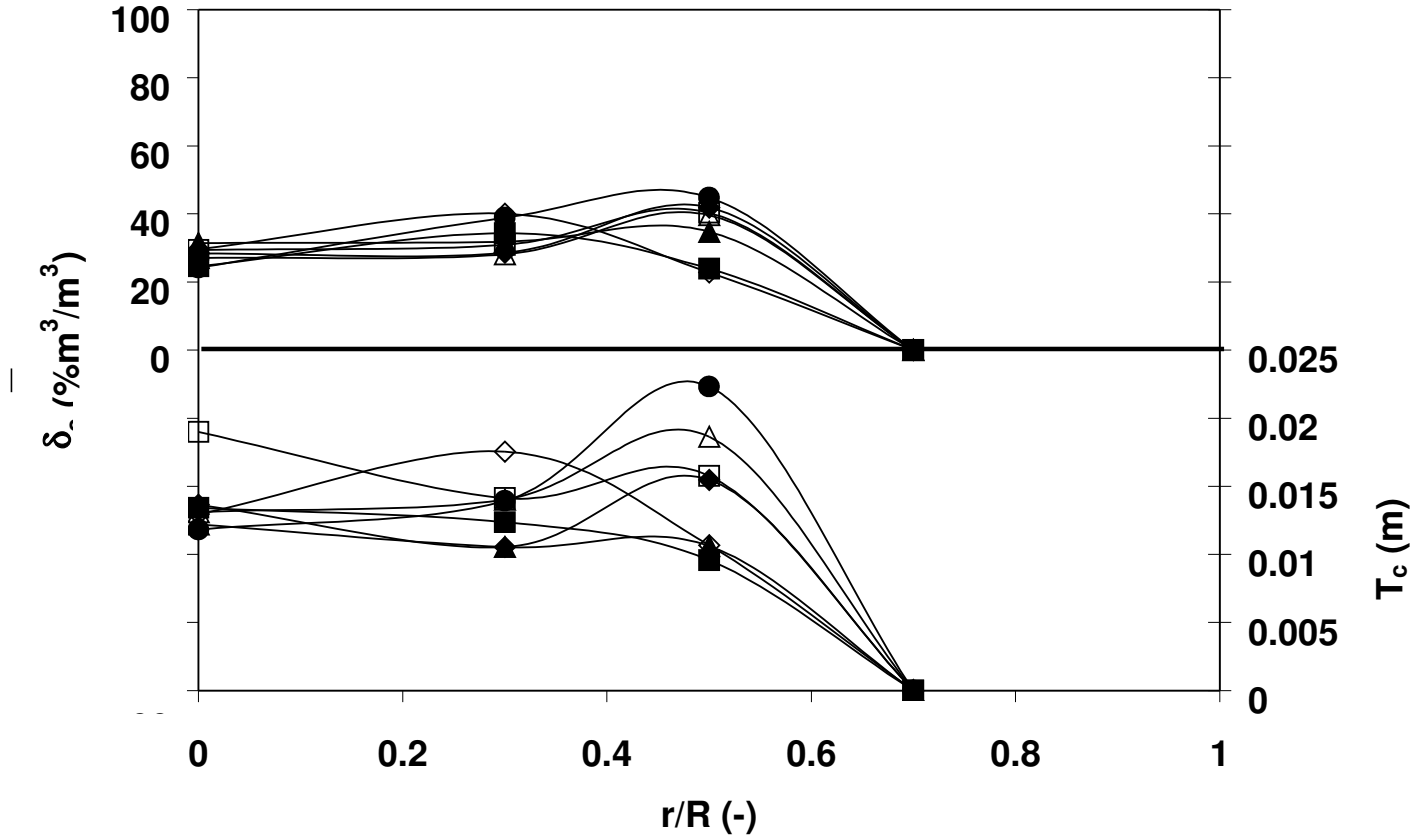

Figure 10: Radial profiles of the fraction and the time-averaged thickness of the cloud phase at 30 cm above the distributor (0.2 m/s ■. 0.3 m/s ◆. 0.4 m/s 娚. 0.5 m/s 図. 0.6 m/s 撝. 0.7 m/s 斂. 0.8 m/s △). Effect of the fluidizing velocity, U_f.

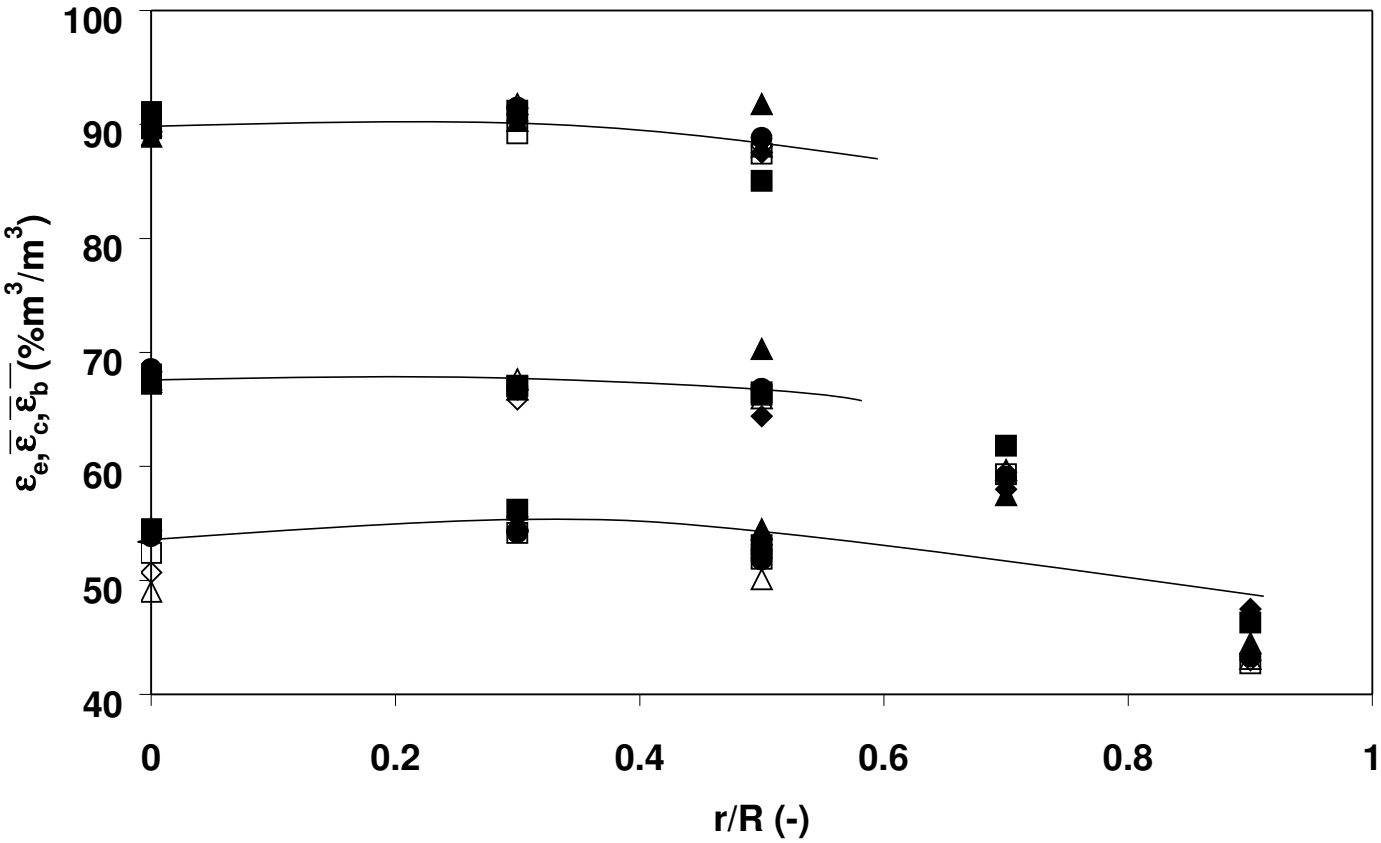

Figure 11 : Radial profiles of the emulsion, the cloud, and the bubble phases time-averaged sporosity, ε_e, ε_c, ε_b, at 30 cm above the distributor (0.2 m/s ■. 0.3 m/s ◆. 0.4 m/s 娉. 0.5 m/s ■. 0.6 m/s 撷. 0.7 m/s 獸. 0.8 m/s △). Effect of the fluidizing velocity, U_f.

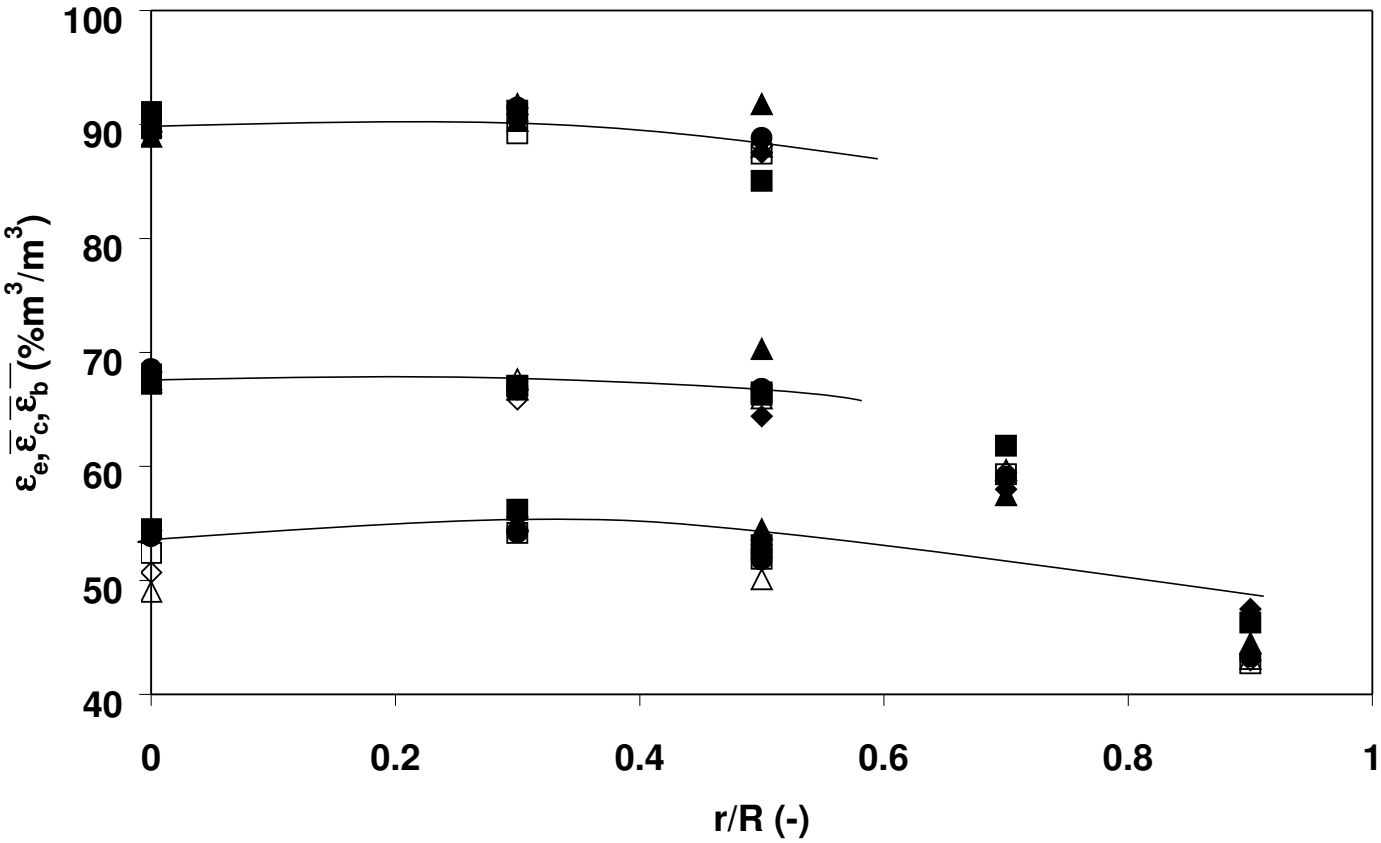

Figure 12 : Radial profiles of the emulsion, the cloud, and the bubble phases time-averaged porosity, ε_e, ε_c, ε_b, at 30 cm above the distributor (0.2 m/s ■. 0.3 m/s ◆. 0.4 m/s ▲. 0.5 m/s ●. 0.6 m/s ▬. 0.7 m/s ♫. 0.8 m/s ▯). Effect of the fluidizing velocity, U_f

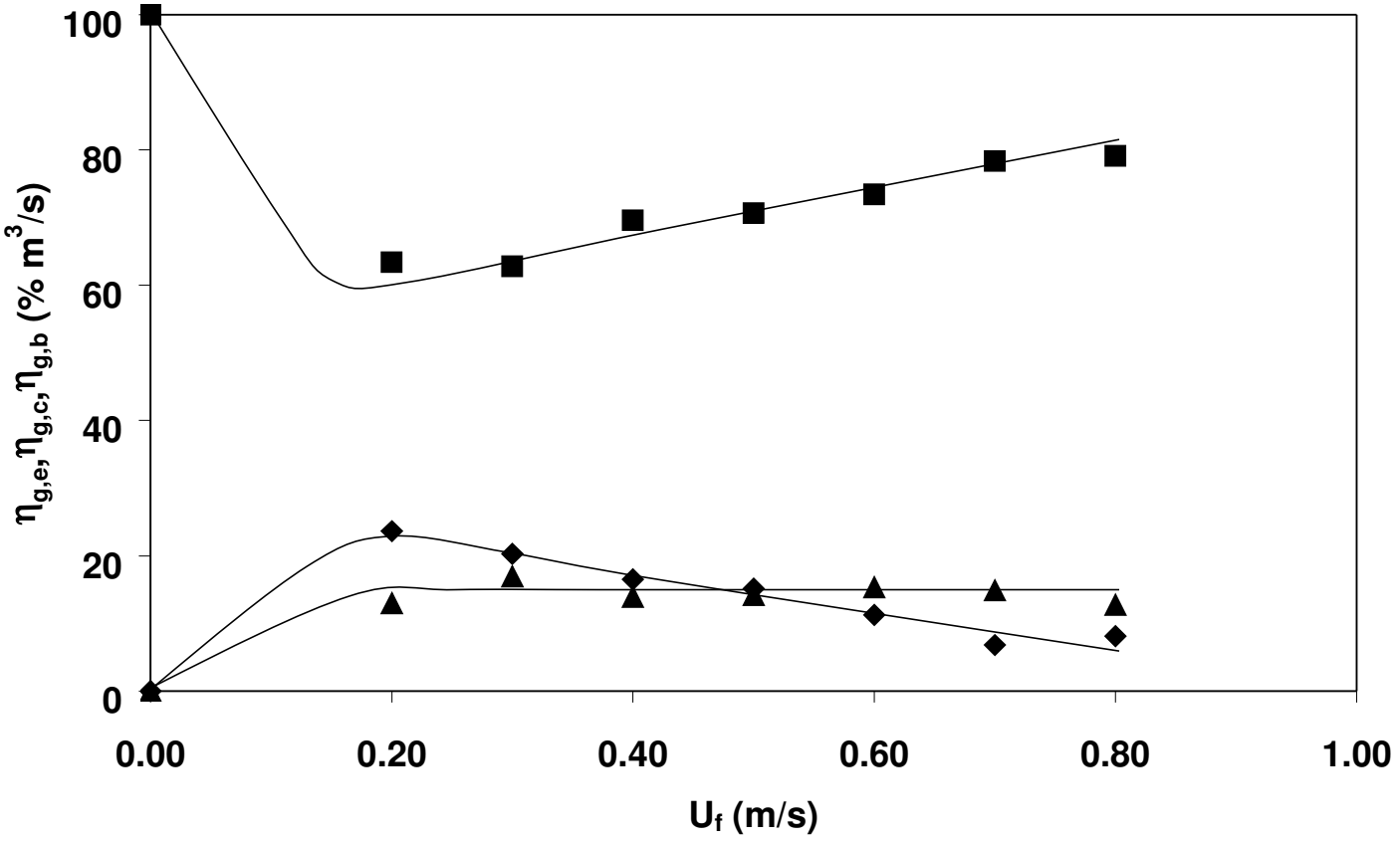

Figure 13 : Fraction of the total gas mass flux through the emulsion-phase, $\eta_{g,e}$ (■), the cloud-phase, $\eta_{g,c}$, (◆), and the bubble-phase, $\eta_{g,b}$, (▲) at 30 cm above the distributor. Effect of the fluidizing velocity, U_f.

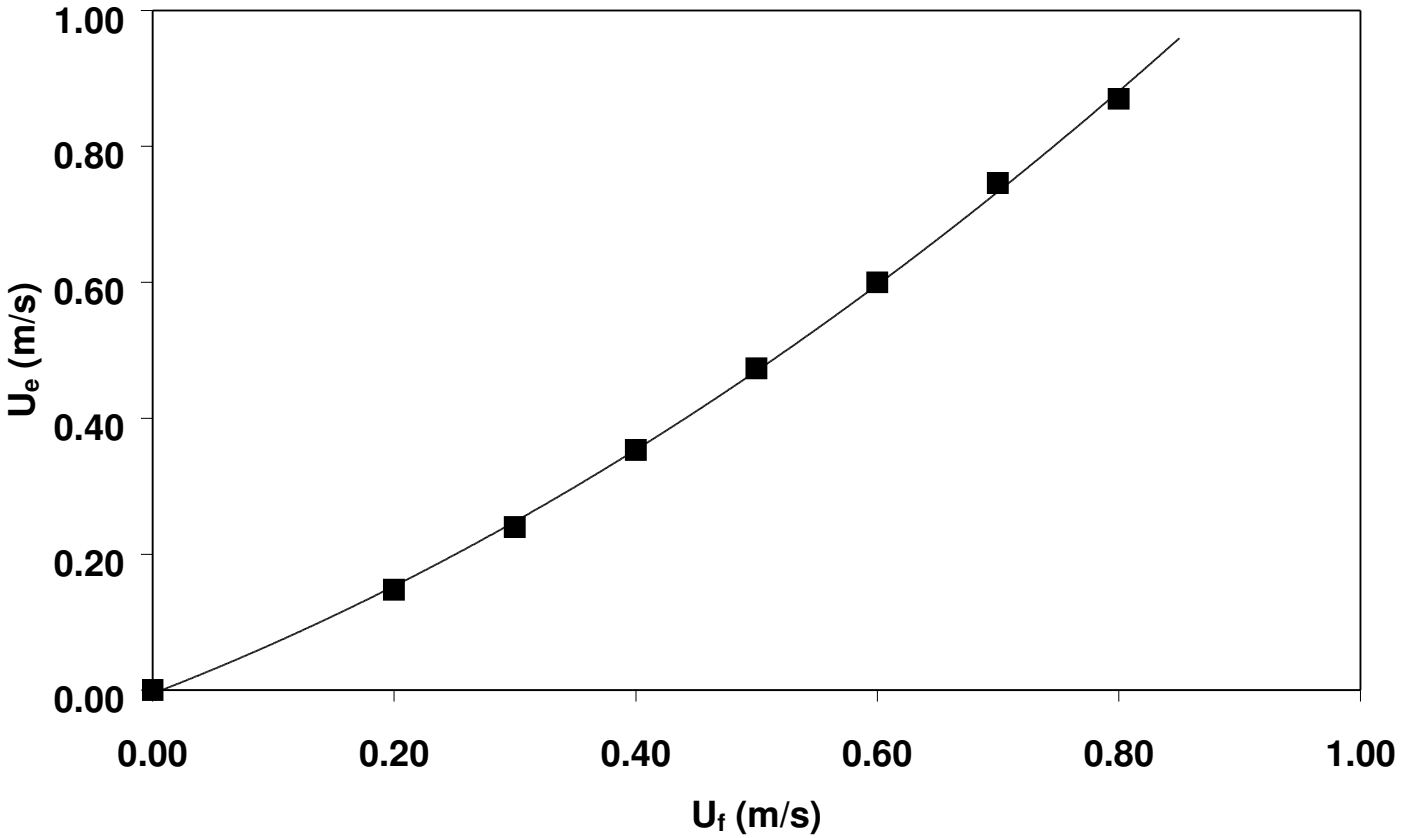

Figure 14: Superficial gas velocity in the emulsion, $\overline{U_e}$. Effect of the fluidizing velocity, U_f.

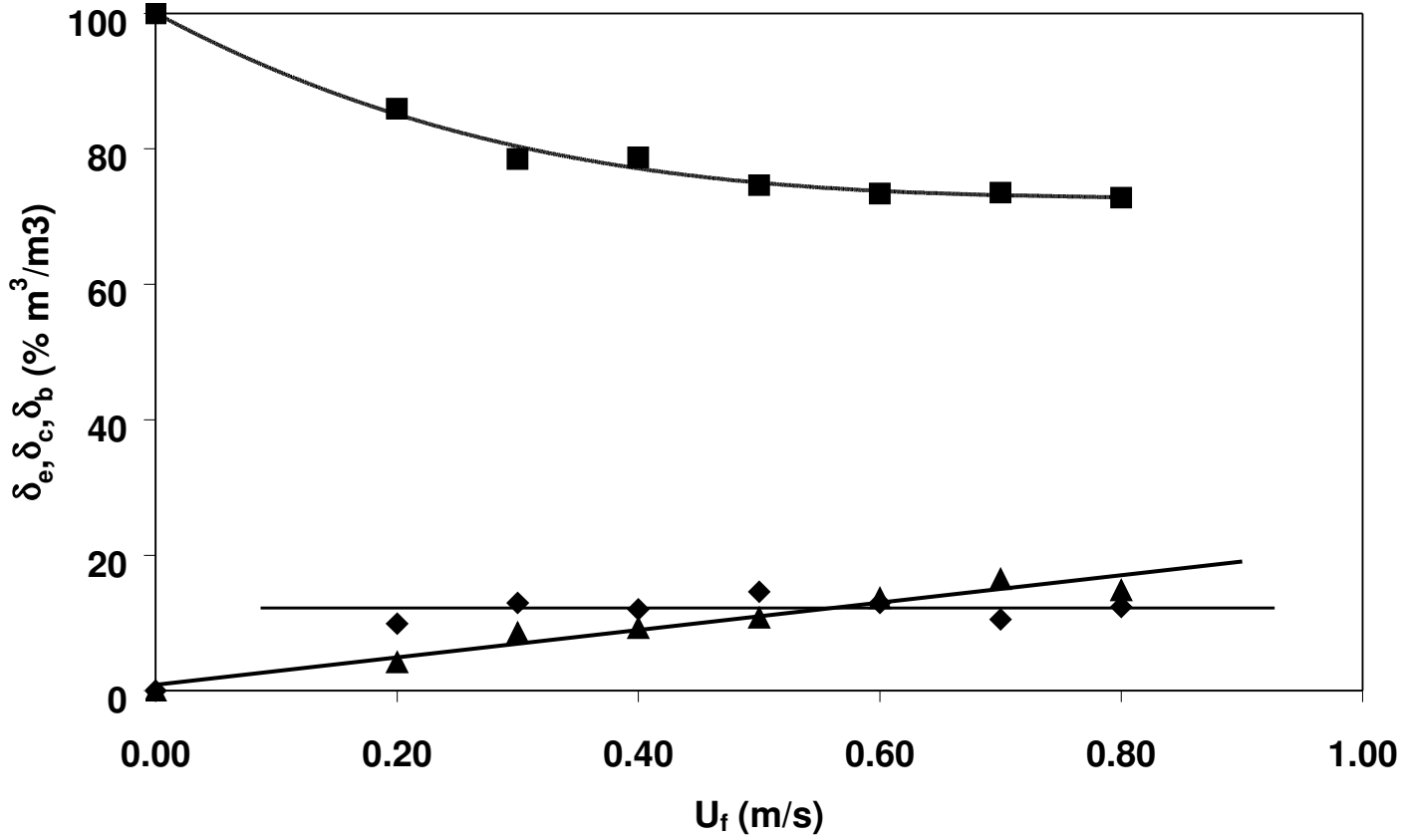

Figure 15: Fraction of the emulsion, $\overline{\delta_e}$ (■), the cloud, $\overline{\delta_c}$ (◆), and the bubble, $\overline{\delta_c}$, phases (▲). Effect of the fluidizing velocity, U_f.

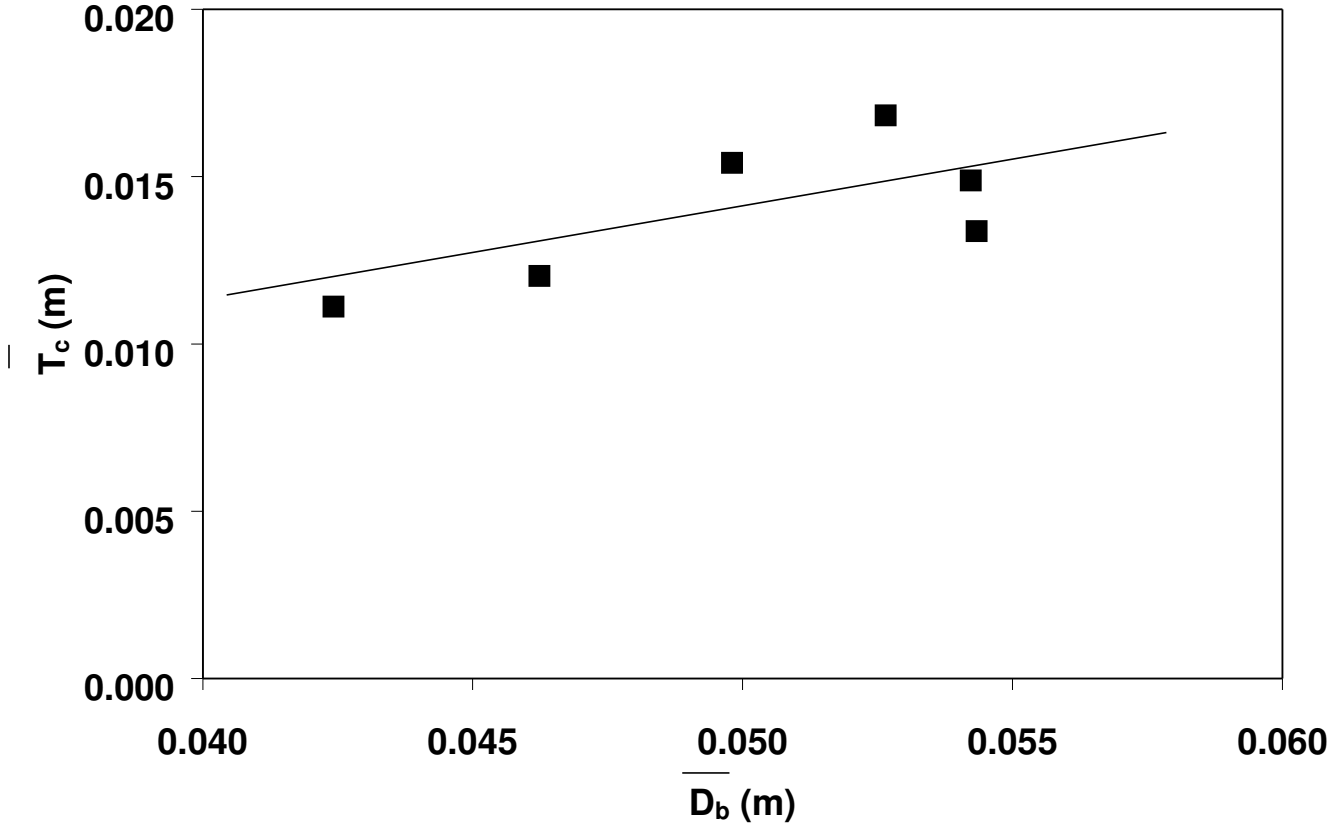

Figure 16 : Relationship between the time-averaged overall cloud thickness, $\overline{T_c}$, and the time-averaged overall bubble chord, $\overline{U_b}$.

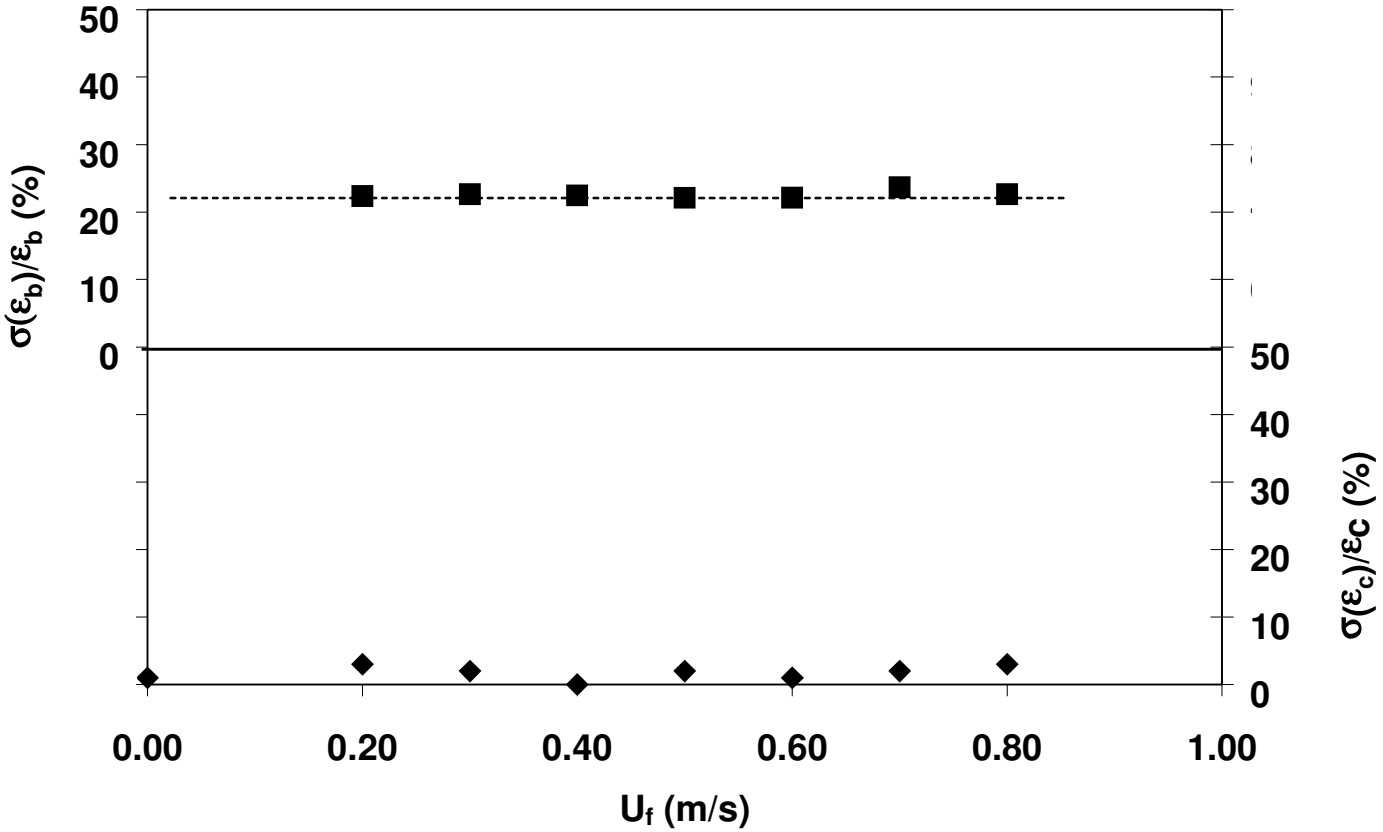

Figure 17 : Relative standard deviation of the bubble porosity (■) and cloud porosity (◆). Effect of the fluidizing velocity, U_f.

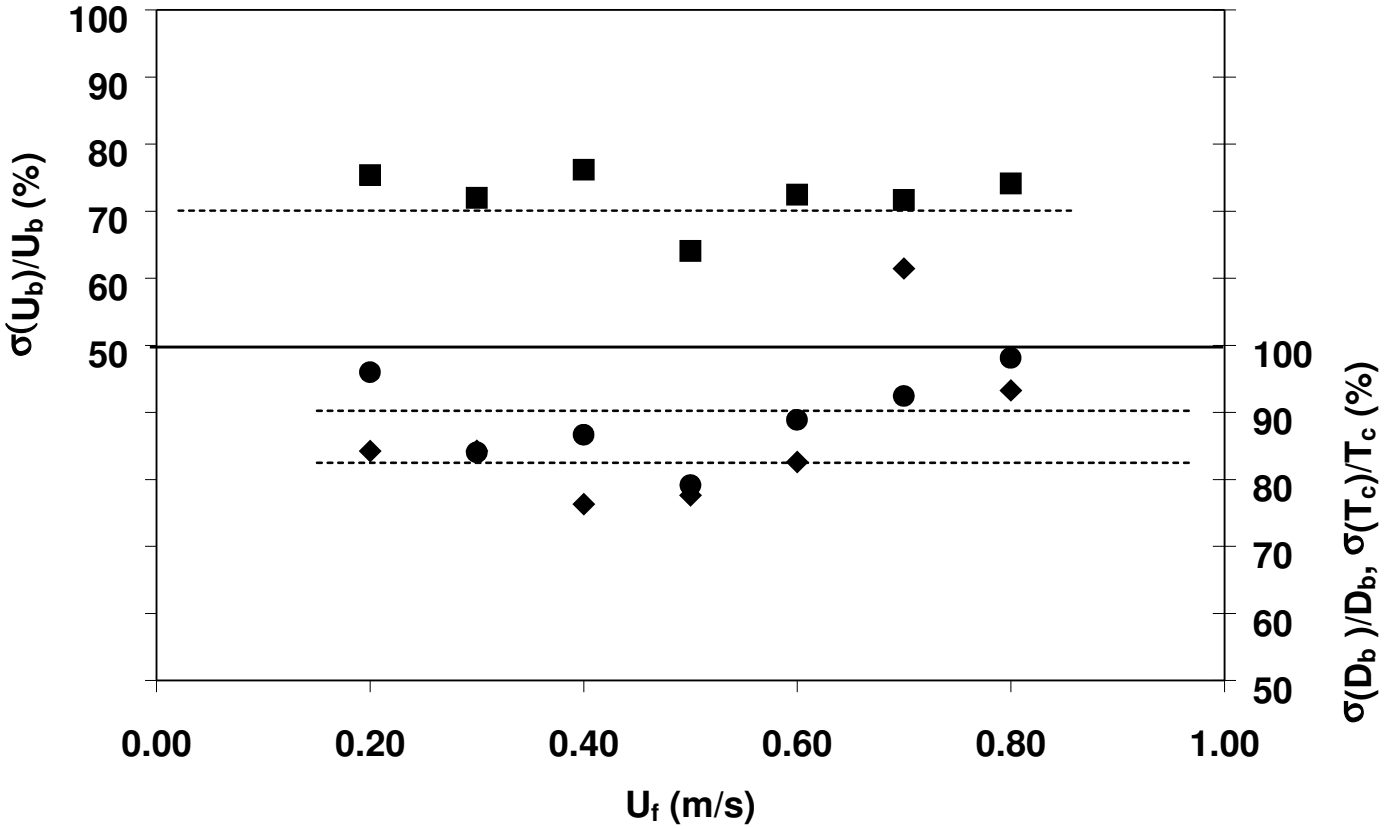

Figure 18 : Relative standard deviation of the bubble velocity (■), bubble chord (●), and cloud thickness (◆). Effect of the fluidizing velocity, U_f.

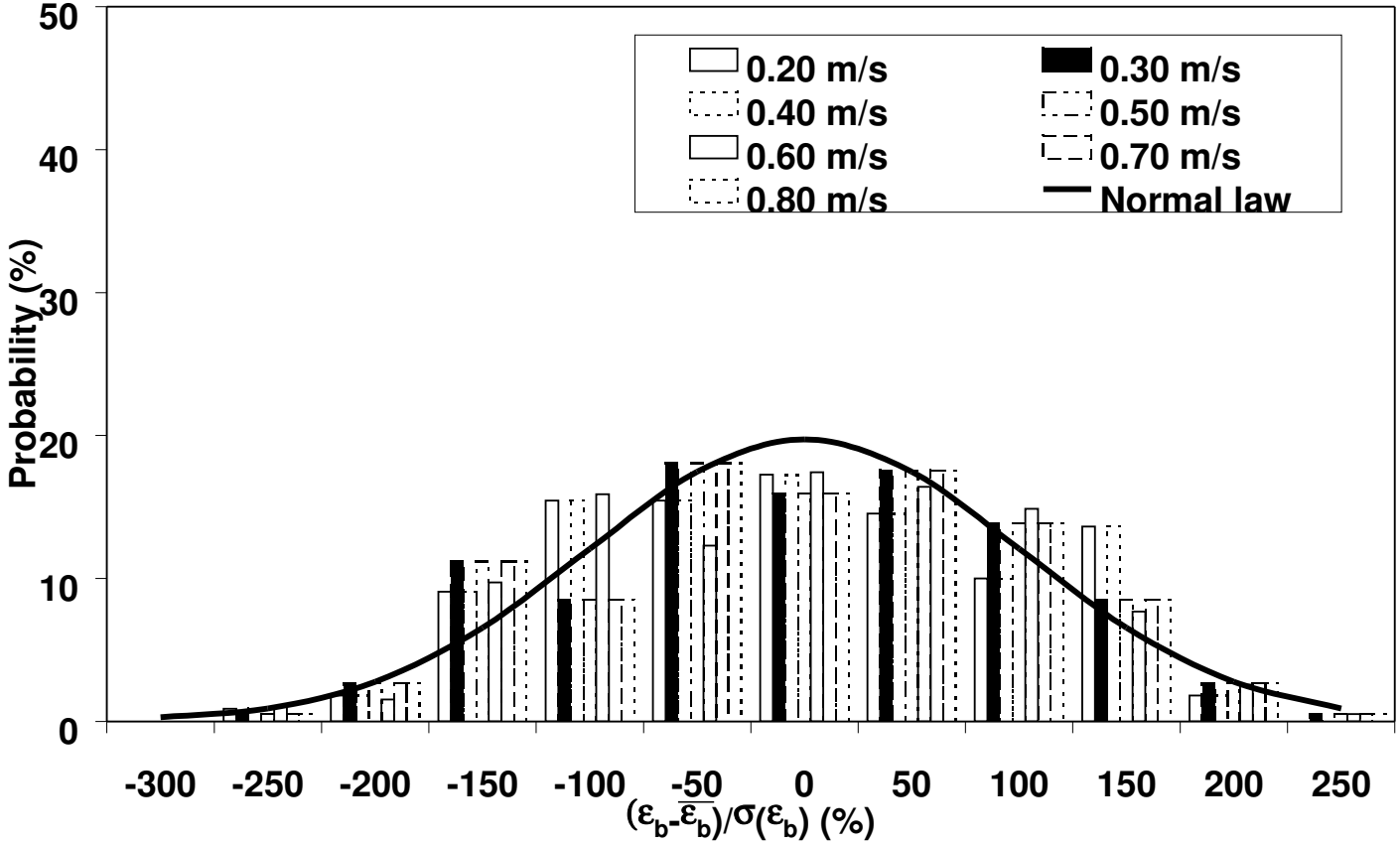

19 : Distribution of the reduced bubble porosity at 30 cm above the distributor. Normal law (—).

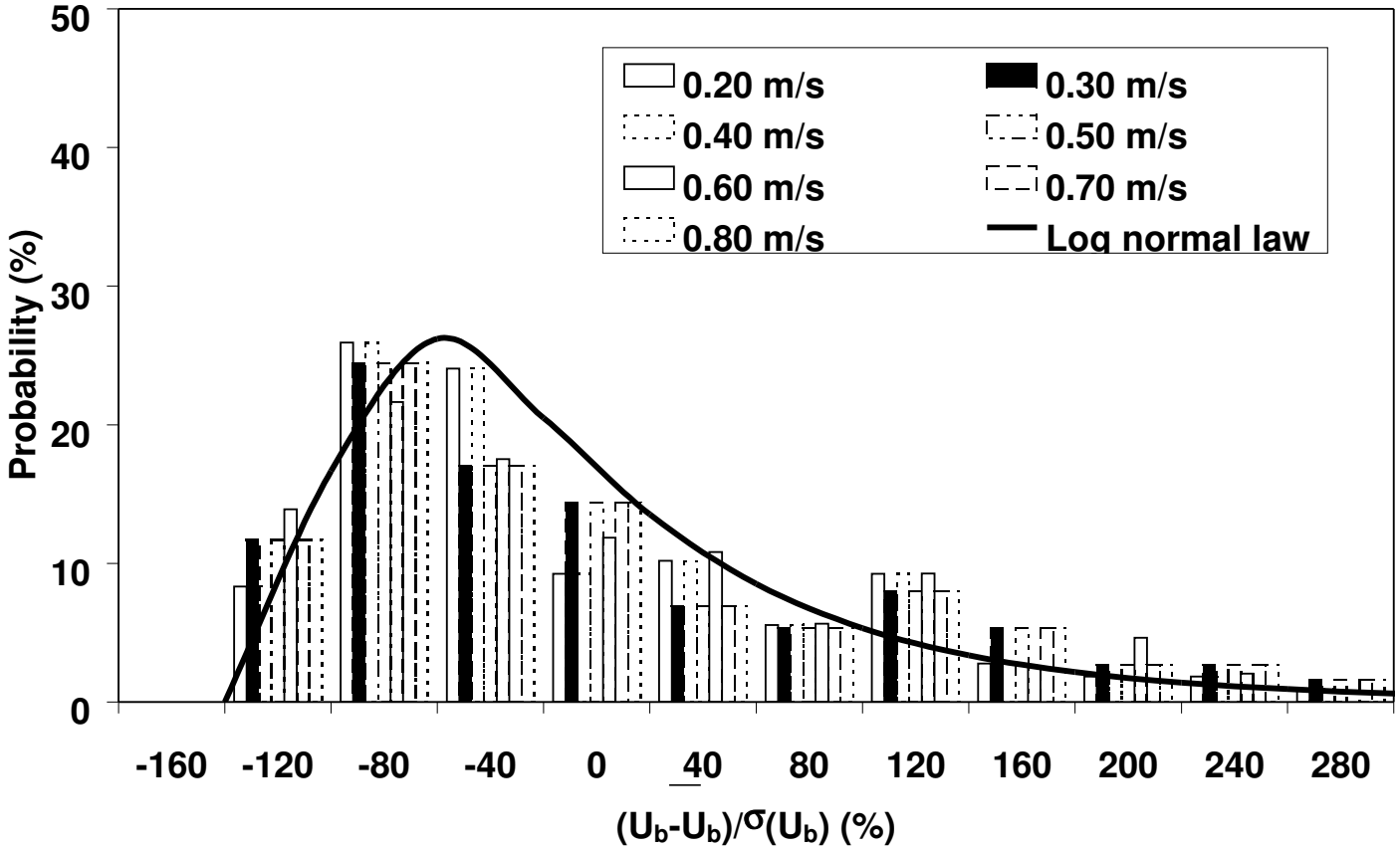

Figure 20 : Distribution of the reduced bubble velocity at 30 cm above the distributor. Lognormal law (—).

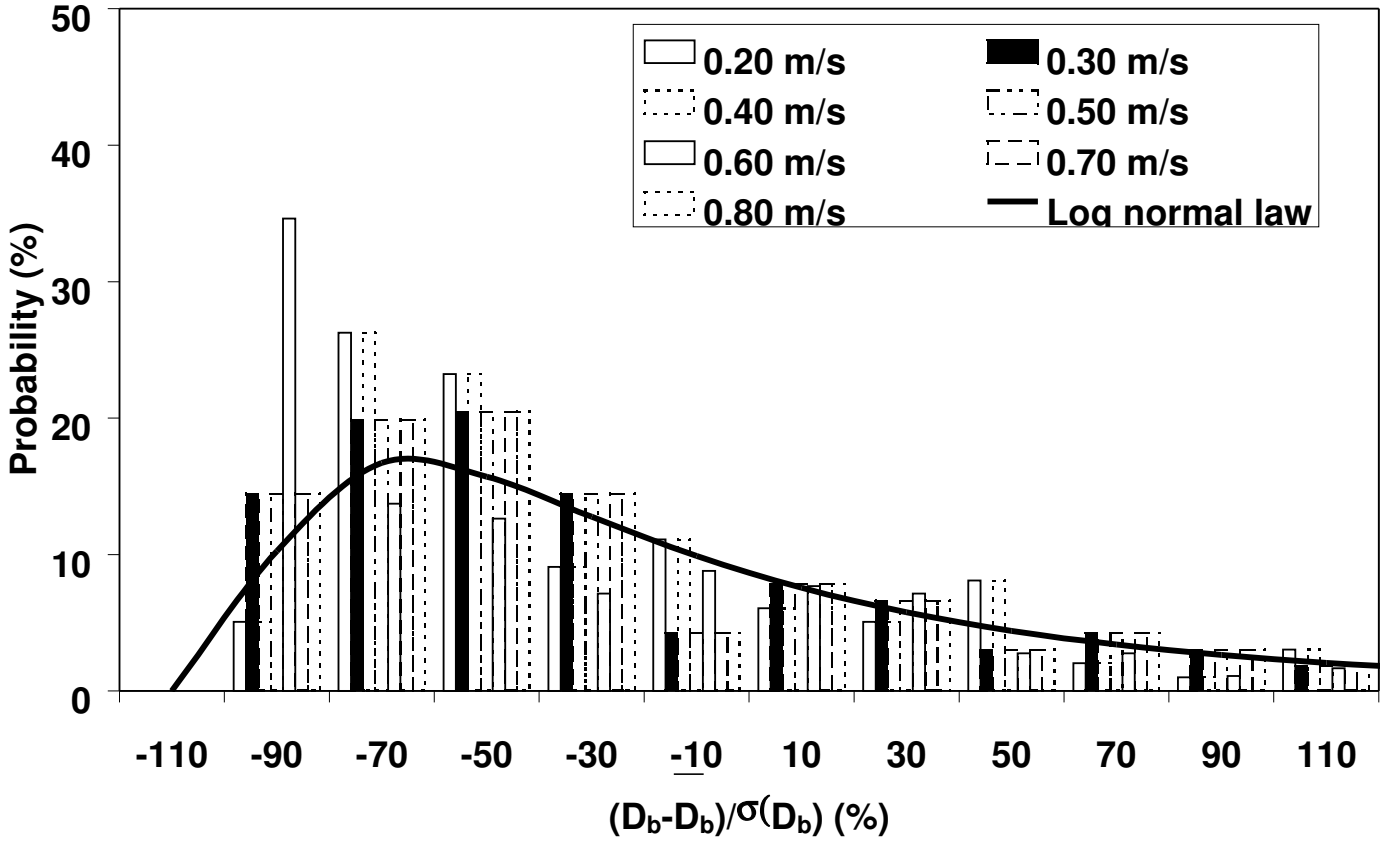

Figure 21 : Distribution of the reduced bubble chord at 30 cm above the distributor. Log normal law (—).

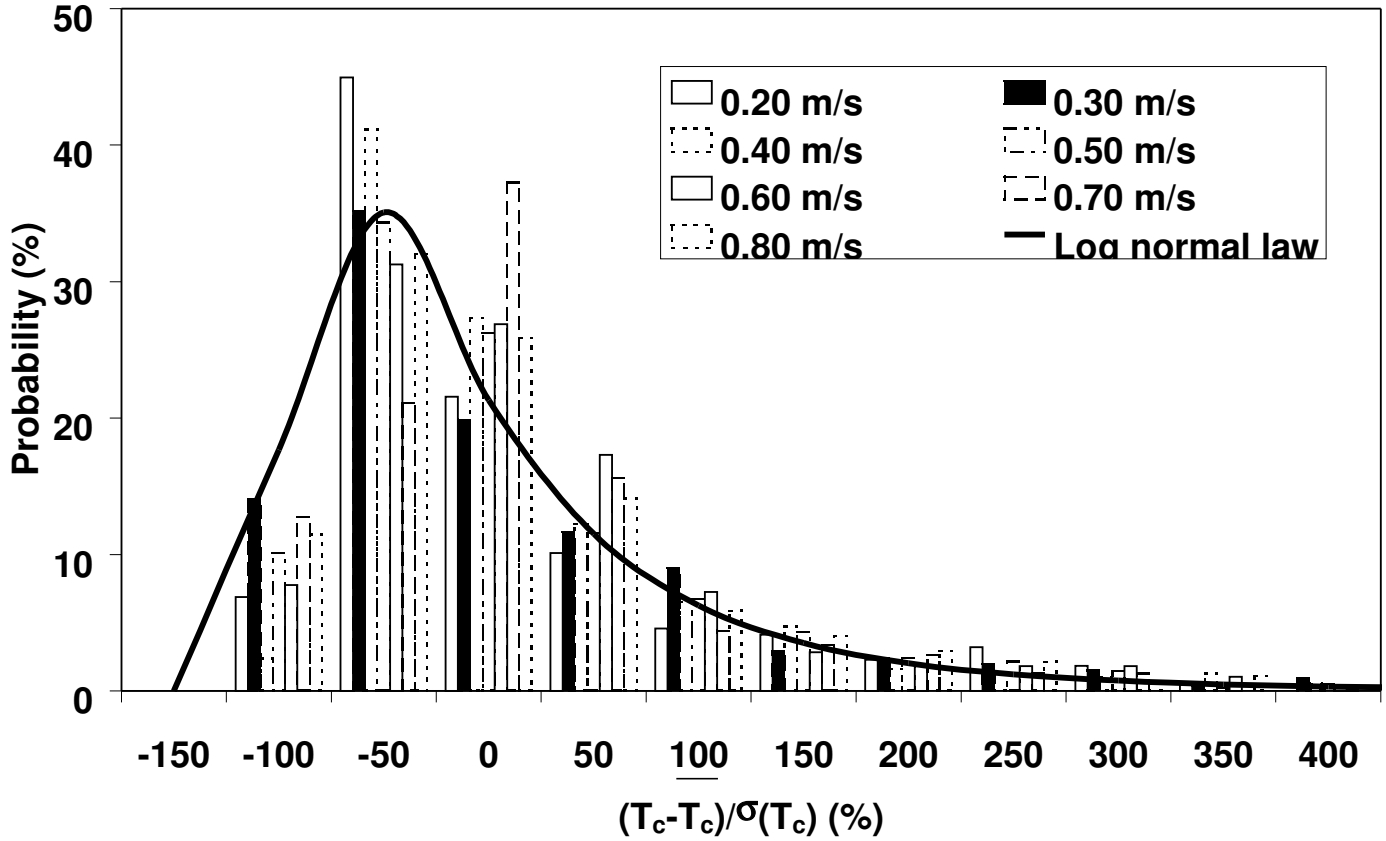

Figure 22 :Distribution of the reduced cloud thickness at 30 cm above the distributor. Log normal law (—).